Perivascular stem cell- loaded photopolymerized methacrylate bone ECM hydrogel in bone regeneration

2022 Orthodontic Faculty Development Fellowships (OFDFA)

Dr. Ginny Ching Yun Hsu

hsug@ohsu.edu
O: 503-494-8565

FollowUp Form

Award Information

In an attempt to make things a little easier for the reviewer who will read this report, please consider these two questions before this is sent for review:

- *Is this an example of your very best work, in that it provides sufficient explanation and justification, and is something otherwise worthy of publication? (We do publish the Final Report on our website, so this does need to be complete and polished.)*

- *Does this Final Report provide the level of detail, etc. that you would expect, if you were the reviewer?*

Title of Project*

Perivascular stem cell- loaded photopolymerized methacrylate bone ECM hydrogel in bone regeneration

Award Type

Orthodontic Faculty Development Fellowship Award (OFDFA)

Period of AAOF Support

July 1, 2022 through June 30, 2023

Institution

Oregon Health & Science University

Names of principal advisor(s) / mentor(s), co-investigator(s) and consultant(s)

Laura Iwasaki, Luiz Bertassoni

Amount of Funding

$20,000.00

Abstract

(add specific directions for each type here)

As an Orthodontist-scientist, my career goals are to establish myself as an independent investigator in the field of craniofacial bone biology to make significant contributions to advance the field of Orthodontics. Currently, I am an Assistant Professor in the Department of Orthodontics at Oregon Health & Science University (OHSU). In this American Association of Orthodontists Foundation (AAOF), Orthodontics Faculty

Development Fellowship Award (OFDFA) application, I have included detailed Educational, Research, Teaching and Clinical Skills Plans with the primary emphasis on the Research Plan. These four developmental plans are essential for my career development as an orthodontist, researcher, and educator.

Of my 5-day per week full-time faculty appointment, I have 75% protected research time, per my employment contract and as dictated by my K08 Clinical Investigator Award from the National Institutes of Health (NIH). This research time will be devoted to the Research Plan described herein, plus efforts to utilize this project's outcomes as a basis for writing manuscripts and grant applications. The rest of my work week will be dedicated as follows: 10% to the Teaching Plan, 10% to the Clinical Skills Plan, and 5% to the Educational Plan.

My interests in craniofacial development and regeneration led to the proposed research project: "Perivascular stem cell-loaded photopolymerized methacrylate bone ECM hydrogel in bone regeneration" Craniofacial skeletal non-healing bone defects such as cleft palate or extensive critical size wound defects remain a significant problem in orthopedic treatment, accompanied individual hardships and societal burdena. Besides the defect size, poor local stem cell numbers, functions or patients' healing abilities are also potential challenges during healing processes. This project will test the working hypotheses that (1) optimized Perivascular stem cells (PSCs)distribution and graft stiffness will significantly improve osteogenic differentiation and vascularization in mouse calvarial defect healing and (2) result in a superior bone-forming efficacy with improved safety profile compared to current standards for care. Specifically, the two aims of this project are:

Aim 1: Optimize optimized light-emitting diode (LED) photopolymerized methacrylate bone extracellular matrix hydrogel (BoneMA) (LP-BoneMA) and cell homogeneity for osteogenic PSCs to formulate Bone-Gel.
Aim 2: Apply Bone-Gel to Critical-size Mouse Calvarial Defect Model.

I anticipate presenting the results from the proposed project at the 2023 American Association of Dental Research (AADR) Annual Session and generating at least one publication as corresponding author in a peer-reviewed journal with a high impact factor (>5), such as Biomaterials or Stem Cell Translational Research. This research will generate preliminary data for future R01 or R21 grant applications to the NIH, focused on mineralization tissue regeneration. Ultimately, I will combine my experience and knowledge with translational research skills and bring the bench work to the chairside.

My advisors Drs. Iwasaki and Bertassoni each have strong records of mentoring clinician-scientists. I will continue to work closely with them. In particular, during the award period we will meet monthly to review the progress and outcomes of my career development plans.

Respond to the following questions:

Detailed results and inferences:*

If the work has been published, please attach a pdf of manuscript below by clicking "Upload a file".
OR
Use the text box below to describe in detail the results of your study. The intent is to share the knowledge you have generated with the AAOF and orthodontic community specifically and other who may benefit from your study. Table, Figures, Statistical Analysis, and interpretation of results should also be attached by clicking "Upload a file".

compressed.pdf

Were the original, specific aims of the proposal realized?*

Yes, we completed all the aims and further validated the markers in depth.

Were the results published?*

Yes

Have the results of this proposal been presented?*

Yes

To what extent have you used, or how do you intend to use, AAOF funding to further your career?*

AAOF OFDFA is a critical funding source for projects that are relevant to our specialty. My OFDFA from AAOF is allowing me not only attending meetings and courses to horning my educational, clinical and research skills but also to generate preliminary data and publications to prepare NIH grant application.

Accounting: Were there any leftover funds?

$0.00

Published

Citations*

You indicated results have been published. Please list the cited reference/s for publication/s including titles, dates, author or co-authors, journal, issue and page numbers

1.Thottappillil N, Gomez-Salazar M, Xu M, Qin Q, Xing X, Xu J, Broderick K, Yea J, Archer M, Hsu GC, Péault B, James AW. ZIC1 dictates osteogenesis versus adipogenesis in human mesenchymal progenitor cells via a Hedgehog dependent mechanism. Stem Cells. Forthcoming.
2. Lu AZ, Chandra D, Chandra SR, James AW, Hsu GC. Differential pericyte marker expression in craniofacial benign and malignant vascular tumors. Journal of Oral Pathology and Medicine. Forthcoming.
3. Hsu GC, Wang Y, Lu AZ, Gomez-Salazar MA, Xu J, Li D, Meyers C, Negri S, Wangsiricharoen S, Broderick KP, Peault B, Morris CD, James AW. TIAM1 acts as an actin organization regulator to control adipose-derived pericyte cell fate. JCI Insight. 2023 May 23;. doi: 10.1172/jci.insight.159141. [Epub ahead of print] PubMed PMID: 37219951.
4. Hsu GC. Challenges and Perspectives on the Use of Pericytes in Tissue Engineering. Current Tissue Microenvironment Reports. 2022 May. doi: https://doi.org/10.1007/s43152-022-00039-2.

Was AAOF support acknowledged?

If so, please describe:

Yes

Presented

Please list titles, author or co-authors of these presentation/s, year and locations:*

ZIC1 dictates osteogenesis versus adipogenesis in human progenitor cells via a Hedgehog dependent mechanism. Neelima Thottappillil, Ph.D., Mario Gomez-Salazar, Ph.D., Mingxin Xu M.D., Ph.D., Mary Archer, B.S, Kristen Broderick, M.D., Bruno Péault, Ph.D., Ginny Ching-Yun Hsu B.D.S., M.S., Aaron W. James, M.D., Ph.D. 2022 ASBMR. Austin, Texas, USA.

Differential pericyte marker expression in craniofacial benign and malignant vascular tumorsAmy Z. Lu, B.S. Dave Chandra D.D.S., Ph.D., Srinivasa R. Chandra, M.D., B.D.S., FDS, FIBCSOMS., Aaron W. James M.D., Ph.D., Ginny Ching-Yun Hsu B.D.S., M.S. 2022 OHSU SOD Research Day, Portland, Oregon

Was AAOF support acknowledged?

If so, please describe:

Yes

Internal Review

Reviewer Comments

Reviewer Status*

File Attachment Summary

Applicant File Uploads

- compressed.pdf

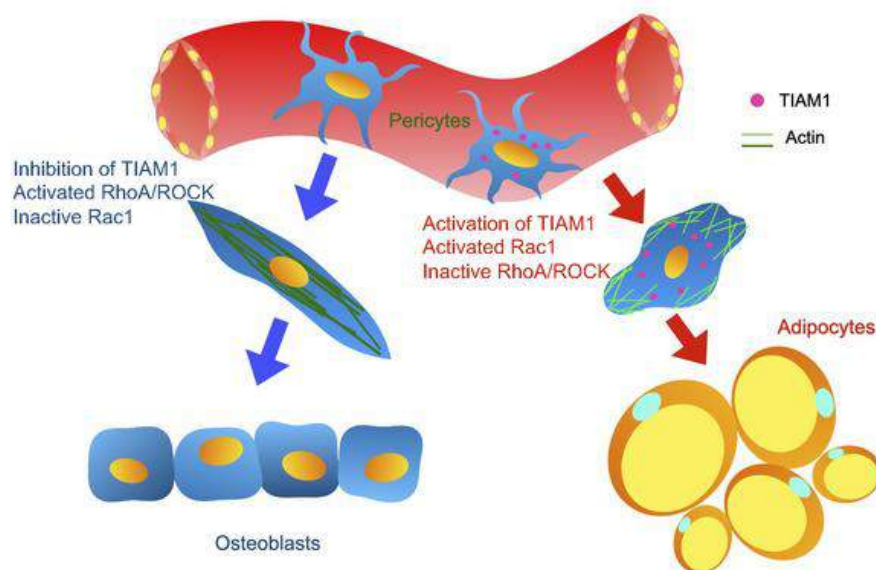2022 Orthodontic Faculty Development Fellowships
(OFDFA)

TIAM1 acts as an actin organization regulator to control adipose-derived pericyte cell fate

Ginny Ching-Yun Hsu, … , Carol D. Morris, Aaron W. James

Research   In-Press Preview   Bone biology   Cell biology

Graphical abstract

1 TIAM1 acts as an actin organization regulator to control adipose-derived pericyte cell
2 fate
3

4 Ginny Ching-Yun Hsu B.D.S., M.S.[1,2], Yiyun Wang, Ph.D.[1], Amy Z. Lu, B.S.[1], Mario A.

5 Gomez-Salazar, Ph.D.[1], Jiajia Xu, Ph.D.[1], Dongqing Li, Ph.D.[1], Carolyn Meyers, B.S.[1],

6 Stefano Negri, M.D.[1], Sintawat Wangsiricharoen, M.D.[1], Kristen Broderick, M.D.[3], Bruno

7 Peault, Ph.D.[5,6], Carol Morris, M.D.[4], Aaron W. James, M.D., Ph.D.[1]*

8

9 [1] Departments of Pathology, [3] Plastic Surgery, and [4] Orthopaedic Surgery, Johns

10 Hopkins University, 21205; [2] Oregon Health & Science University; [4] Center for

11 Cardiovascular Sciences, University of Edinburgh, Edinburgh, United Kingdom; [5] UCLA

12 and Orthopaedic Hospital Department of Orthopaedic Surgery and the Orthopaedic

13 Hospital Research Center, 90095 [6]

14 -

15 * Correspondence: Aaron W. James, M.D., Ph.D., Department of Pathology, Johns

16 Hopkins University, Ross Research Building, Room 524A, 720 Rutland Avenue,

17 Baltimore MD 21205; Tel: (410) 502-4143; Fax: (410) 955-0394; Email:

18 awjames@jhmi.edu

19

20

21

22

23

24 **Abstract**

25 Pericytes are multipotent mesenchymal precursor cells that demonstrate tissue-specific

26 properties. In this study, by comparing human adipose and periosteal-derived pericyte

27 microarrays, we identified TIAM1 as a key regulator of cell morphology and differentiation

28 decisions. TIAM1 represents a tissue-specific determinant between predispositions for

29 adipocytic versus osteoblastic differentiation in human adipose-derived pericytes. *TIAM1*

30 overexpression promotes an adipogenic phenotype, whereas its downregulation

31 amplifies osteogenic differentiation. These results were replicated *in vivo* xenograft

32 animal model, in which *TIAM1* misexpression altered bone or adipose tissue generation

33 in an intramuscular xenograft animal model. Changes in pericyte differentiation potential

34 induced by *TIAM1* misexpression correlated with actin organization and altered

35 cytoskeletal morphology. Small molecule inhibitors of either Rac1 or RhoA/ROCK

36 signaling reversed TIAM1-induced morphology and differentiation in pericytes. In

37 summary, our results demonstrate that TIAM1 regulates the cellular morphology and

38 differentiation potential of human pericytes, representing a molecular switch between

39 osteogenic and adipogenic cell fates.

40

Introduction

Pericytes have mesenchymal stem cell (MSC)-like properties, including multipotentiality, immunoregulatory functions, and diverse roles in tissue repair (1-3). A general hypothesis holds that pericytes function as tissue-specific progenitor cells during tissue regeneration (4). For example, skeletal pericytes can differentiate into osteoblasts, while smooth muscle-derived pericytes do not (5). Likewise, cord blood mesenchymal progenitors are more multipotent than postnatal bone marrow MSCs to undergo osteogenic differentiation, chondrogenesis and adipogenesis (6). Pericytes derived from tissue around the joint demonstrate heightened chondrogenic potential (7). Important examples of heterologous differentiation of pericytes are also reported, and our group has focused on 'adipose-to-bone' transdifferentiation of human pericytes (reviewed in (8)). Further exploration of human pericytes as tissue-specific progenitors and the cell- and context-specific permissive situations for heterologous differentiation have important implications for cell biology and the use of pericytes in cell therapy.

In previous work, we examined the tissue-specific properties of human pericytes by directly comparing pericytes from skeletal (periosteal) and adipose tissue sources (4). Results showed that CD146$^+$Lin$^-$ skeletal pericytes preferentially mineralized and ossified, whereas CD146$^+$Lin$^-$ adipose tissue pericytes preferentially formed adipocytes (4). Using transcriptomic analysis, we investigated osteogenesis-related signaling pathways and differentially expressed genes (DEGs) in pericytes from each tissue depot. Among other findings, we identified a subset of CXCR4-expressing pericytes in adipose tissue that

63   displayed osteoprogenitor cell attributes (4). Due to these results, it has been suggested

64   that specific genes and pathways maintain tissue-specific potential.

65

66   In the present study, we addressed the question of whether endogenous factors or

67   signaling pathways within human adipose tissue pericytes restrain their ability to ossify.

68   We reasoned that basal signaling pathways that actively inhibit osteogenic pathways may

69   be present among adipose tissue pericytes *in vivo*. To this end, transcriptomic data of

70   skeletal versus soft tissue CD146$^+$ human pericytes were reanalyzed to identify

71   differences among many pathways related to cytoskeletal organization and Rho GTPase

72   signaling. From these differentially expressed genes, TIAM1 (T-cell lymphoma invasion

73   and metastasis 1) was chosen as a novel candidate. TIAM1 is a guanine nucleotide

74   exchange factor (GEF) and can specifically regulate the Rho family of small GTPases

75   (Rac, Rho and Cdc42), including Rac1 (9). TIAM1 has been studied in contexts related

76   to cell migration, adhesion, and proliferation by controlling actin remodeling (10, 11),

77   which in turn is known to influence mesenchymal progenitor cell differentiation (12, 13).

78

79   Here, we employed a detailed examination of TIAM1 expression within human pericytes.

80   Briefly, we observed that *TIAM1* misexpression alters pericyte cellular morphology

81   leading to skewed osteo/adipogenic differentiation via changes in the reciprocal

82   relationship of Rac1 and RhoA/ROCK signaling. This data was recapitulated after

83   xenotransplantation in mice. By using Rac1 or RhoA/ROCK signaling small molecular

84   inhibitors NSC23766 or Y27632, the reverse changes in pericyte morphology and

85   differentiation were observed. This data demonstrates that TIAM1 directs cell

86 differentiation, an important feature in human pericytes that may explain tissue-intrinsic

87 differences in this progenitor cell type.

88

89 **Results**

90 **TIAM1 is enriched within adipose tissue-derived pericytes**

91 To investigate tissue-specific gene expression of pericytes, human adipose and

92 periosteal pericyte were FACS sorted to obtain CD146$^+$CD31$^-$CD45$^-$ cell preparations

93 **(Supplemental Fig. S1)**(4)**.** A clear separation between gene expression profiles was

94 observed when comparing periosteal and adipose pericytes, as revealed by principal

95 component analysis **(Fig. 1A).** Gene Ontology (GO) re-analysis revealed changes in

96 terms related to cell size, shape, and spreading between adipose and periosteal

97 pericytes. For example, enrichment in genes associated with "Cell Polarization" were

98 identified among periosteal pericytes **(Fig. 1B, Supplemental Table S4).** On the other

99 hand, GO terms such as "Cell Spreading" were enriched in adipose tissue-derived

100 pericytes **(Fig. 1C, Supplemental Table S5)**. Ingenuity Pathway Analysis (IPA) showed

101 a series of Rho GTPase-related cytoskeletal pathways that were differentially activated

102 within adipose versus periosteal CD146$^+$ pericytes, such as the RhGDI pathway, RhoA

103 and Rac signaling pathways, as well as terms such as Actin cytoskeletal signaling

104 **(Fig. 1D**, red boxes**)**. Among single genes involved in Rho GTPase-related signaling, the

105 Rho regulator TIAM1 showed enriched in expression across adipose tissue-derived, but

106 not skeletal-derived pericytes **(Fig. 1E).**

107

108   TIAM1 (T-lymphoma invasion and metastasis) is a main regulator of the Rho proteins

109   connecting extracellular signals to cytoskeletal modifications (14-18). For instance,

110   TIAM1 regulates integrin-mediated cell-matrix adhesion, E-cadherin cell adhesion, and

111   cell polarity (11, 19). Differential gene expression of *TIAM1* in separately derived human

112   pericyte   samples   was   confirmed   by   qRT-PCR   **(Fig. 1F)**.   Results   from

113   immunohistochemical staining of TIAM1, pericyte markers CD146 and α-SMA, and

114   endothelial marker CD31 showed that TIAM1 was enriched in adipose tissue pericytes,

115   which was confirmed by a high degree of overlap between TIAM1 and known pericyte

116   markers (CD146 and α-SMA) (**Fig. 1G, H**). Results showed that TIAM1 was enriched in

117   adipose tissue pericytes, which was confirmed by a high degree of overlap between

118   TIAM1 and known pericyte markers (CD146 and α-SMA) (**Fig. 1G**). In contrast,

119   immunohistochemical staining of blood vessels in human periosteal tissues revealed a

120   relatively limited TIAM1 immunoreactivity among bone-associated pericytes (**Fig. 1H**).

121

122   **TIAM1 regulates adipogenic versus osteogenic cell fates among human pericytes**

123   Data demonstrated that *TIAM1* expression decreased across timepoints in osteogenic

124   medium **(Fig. 2A,** blue bars). In contrast, no significant difference in *TIAM1* expression

125   was observed until late adipogenesis, at which time *TIAM1* expression levels were

126   reduced in comparison to undifferentiated cells **(Fig. 2A**, red bars). Next, the effects of

127   *TIAM1* knockdown (KD) on pericyte differentiation were assessed. Validation of siRNA-

128   mediated KD was first performed by qRT-PCR (**Fig. 2B**) and immunocytochemistry and

129   semi-quantitative analysis (**Fig. 2C**). Under osteogenic differentiation conditions, *TIAM1*

130   KD led to an increase in osteogenic gene expression at both 3 and 7 d of differentiation,

131   including Alkaline Phosphatase (ALPL)*, Osteocalcin (BGLAP)*, and *Osterix (SP7)* (**Fig.**

132   **2D**). Consistent with gene expression studies, staining of ALP enzymatic activity was

133   significantly increased with *TIAM1* knockdown at 10 d of differentiation (**Fig. 2E**).

134   Moreover, bone nodule deposition assessed by Alizarin Red (AR) staining and

135   photometric quantification showed a robust increase in the mineralization of cells

136   with *TIAM1* KD **(Fig. 2F).** In contrast, *TIAM1* KD demonstrated opposing effects on

137   adipogenic differentiation of human pericytes (**Fig. 2G, H**). This included significantly

138   decreased expression of adipogenic differentiation markers by qRT-PCR, including

139   *peroxisome proliferator-activated receptor gamma (PPARG)* at 3 d, as well as CCAAT

140   Enhancer Binding Protein Alpha (*CEBPA)* and *fatty acid-binding protein 4 (FABP4)* at 7

141   d of adipogenic differentiation (**Fig. 2G**). Likewise, *TIAM1* KD led to reduced intracellular

142   lipid droplets as visualized by Oil red O staining (**Fig. 2H**). Changes in differentiation

143   potential with *TIAM1* KD were not accompanied by changes in proliferation, as observed

144   by MTS assays (**Supplemental Fig. 2A**).

145

146   Transfection of a CMV plasmid used to promote *TIAM1* overexpression led to a 250-fold

147   upregulation of *TIAM1* expression by qRT-PCR (**Fig. 3A**), which was confirmed by

148   immunocytochemical staining and quantification (**Fig. 3B**). *TIAM1* overexpression in

149   pericytes under osteogenic differentiation conditions led to a decrease in the expression

150   of osteogenic gene markers in comparison to the control plasmid (**Fig. 3C**). Inhibition of

151   osteogenic differentiation with *TIAM1* overexpression was confirmed using ALP and

152   Alizarin red staining (**Fig. 3D, E**). *TIAM1* overexpression led to a significant increase in

153   the expression of adipogenic gene markers including *CEBPA*, *FABP4, and PPARG*

154 **(Fig. 3F)**. With *TIAM1* overexpression, Oil Red O staining likewise showed a significant

155 increase in the intracellular accumulation of lipids after 10 d of differentiation **(Fig. 3G).**

156 Changes in differentiation potential with *TIAM1* overexpression were not accompanied by

157 changes in proliferation (**Supplemental Fig. 2B**). In summary, our studies thus far

158 suggest that TIAM1 exerts prominent pro-adipogenic / anti-osteogenic effects in human

159 pericytes without affecting cell proliferation.

160

161 **TIAM1 misexpression alters human pericyte morphology**

162 Silencing of *TIAM1* gene expression led to an elongated and spindled cell morphology in

163 comparison to an siRNA control, visualized using F-actin staining (**Fig. 4A**).   When

164 quantified, *TIAM1* knockdown pericytes showed increased length and decreased width

165 (**Fig. 4B**). Target genes for the Rac1 and RhoA/ROCK signaling were next assessed,

166 including *ARPC2* (Actin Related Protein 2/3 Complex Subunit 2) and *SRF* (serum

167 response factor), respectively (**Fig. 4C**). As expected from its known function in other cell

168 types (20), *TIAM1* silencing led to a significant increase in RhoA/ROCK and reduction in

169 Rac1 gene targets (**Fig. 4C**). Converse experiments were performed in the context of

170 *TIAM1* overexpression (**Fig. 4D-F**). TIAM1 overexpression led to a wider cell shape in

171 human pericytes (**Fig. 4D**), which when quantified by cell, showed an overall reduced cell

172 length and increased cell width, (**Fig. 4E**).   In parallel, *TIAM1* overexpression led to an

173 increase in the Rac1 gene marker *ARPC2* and a significant decrease in *SRF* expression

174 **(Fig. 4F)**. Thus, *TIAM1* gene misexpression alters actin organization and cellular shape

175 in human pericytes, associated with changes in Rac1 / RhoA/ROCK signaling activity.

176

TIAM1 regulates pericyte cytoskeletal remodeling and cellular differentiation via Rac1 and RhoA/ROCK signaling

Next, the Rac1 inhibitor NSC23766 or RhoA/ROCK inhibitor Y27632 were used as treatment to observe pericyte morphology and differentiation potential in the context of *TIAM1* gene misexpression (**Fig. 5**). Cell morphology was first observed in growth medium (**Fig. 5A,B**). Under siRNA control conditions, pericytes treated with NSC23766 demonstrated a spindle cell shape, while pericytes treated with Y27632 demonstrated a round cell shape (**Fig. 5A**). Under *TIAM1* knockdown conditions, cell spindling was amplified under NSC23766-treated conditions, while Y27632 treatment reversed the spindled appearance induced by *TIAM1* silencing (**Fig. 5B**). Recapitulating our prior findings, knockdown of *TIAM1* significantly increased the expression of osteogenic gene markers in human pericytes (**Fig. 5C**). The Rac1 inhibitor NSC23766 further amplified the osteogenic effect of *TIAM1* knockdown, while the RhoA/ROCK inhibitor Y27632 partially or completely reversed this induction of osteogenic gene expression. Mineralization detection by AR staining and photometric quantification further confirmed these significant changes in osteogenic differentiation (**Fig. 5D, E**).

Converse experiments were next performed in the context of *TIAM1* overexpression and adipogenic differentiation with and without small molecule inhibitors (**Fig. 5F-J**). Significant changes in cell shape were observed with the addition of small molecule inhibitors Rac1 or RhoA/ROCK (**Fig. 5F, G**). By specific adipogenic gene expression (**Fig. 5H**) and Oil red O staining and quantification (**Fig. 5I, J**), the Rac1 inhibitor NSC23766 partially or completed reversed an increase in adipogenesis under *TIAM1*

200 overexpression conditions. Conversely, the RhoA/ROCK inhibitor increased

201 adipogenesis under control conditions, and additively increased adipogenic differentiation

202 among *TIAM1* overexpressing pericytes. Thus, co-application of small molecules in the

203 context of TIAM1 misexpression indicate Rac1 and RhoA/ROCK signaling in TIAM1

204 directed differentiation of human pericytes.

205

206 ***TIAM1* misexpression in human pericytes alters tissue generation *in vivo***

207 Pericyte implantation studies were next performed in athymic mice over an 8 week period

208 in the context of *TIAM1* misexpression. A significant increase in bone formation was

209 observed among *TIAM1* knockdown implantation sites, as observed by µCT cross-

210 sectional imaging and reconstructions (**Fig 6A, B**). Quantitative µCT analysis confirmed

211 a significant increase in bone volume (BV) (**Fig. 6C**) and fractional bone volume (BV/TV)

212 (**Fig. 6D**). Histology by H&E staining showed an increase in osteoblast activity within

213 *TIAM1* knockdown implants (**Fig. 6E**). Likewise, immunohistochemistry for the terminally

214 differentiated osteoblast marker Osteocalcin (OCN) demonstrated increased antigen

215 detection among *TIAM1* knockdown implant sites (**Fig. 6F, G**). In these tissue sections,

216 significant co-expression with the Human Nuclear antigen was observed, confirming

217 tissue generation by human cells (**Fig. 6F,H**). Immunohistochemistry for the adipocyte

218 marker Perilipin 1 (Plin1) demonstrated rare staining across tissue sections, which was

219 primarily in control but not *TIAM1* knockdown implantation sites (**Fig. 6H, I**).

220

221   Next, the converse effects of *TIAM1* overexpression in human pericytes on ectopic tissue

222   generation was assessed in the same model (**Fig. 6J-R**). µCT imaging and analysis

223   demonstrated a reduction in bone formation among pCMV-TIAM1 pericyte implant sites,

224   including in cross-sectional imaging (**Fig. 6J**), 3D µCT reconstructions (**Fig. 6K**), and

225   quantitative analysis (**Fig. 6L,M**). H&E staining confirmed the impression that new bone

226   formation was reduced among *TIAM1* overexpression implant sites (**Fig. 6N**). Foci of

227   OCN immunofluorescent staining were present among control implantation sites and

228   greatly reduced among *TIAM1* overexpression conditions (**Fig. 6O, P**). In contrast, the

229   adipocyte marker Plin1 was significantly increased with adipocytes within pCMV-TIAM1-

230   treated implant sites (**Fig. 6Q, R**), and showed notable overlap with Human Nuclear

231   antigen expression. In summary, changes in *TIAM1* expression direct ectopic tissue

232   generation between bone and fat tissue among human pericytes upon transplantation in

233   a mouse model.

234

235   **Discussion**

236   Mesenchymal progenitor cells are widely used for regenerative medicine for different

237   pathologies, including bone conditions. Easily accessible tissues, such as adipose tissue,

238   are one of the main sources of these cells. The inherent differentiation potential of

239   progenitor cells is linked to their tissue of origin (4, 5). For instance, adipose tissue

240   mesenchymal cells, such as pericytes, are prone to become adipocytes, whereas

241   skeletal-derived cells become bone (4). In the present study, the negative osteogenesis

242   (pro-adipogenesis) regulator TIAM1 is identified and its function is suggested to occur

243   through regulating cytoskeletal morphology. Understanding tissue-specific regulators

244   such as TIAM1 will help elucidate the mechanisms of progenitor cells in vivo and improve

245   the use of these cells for therapeutic purposes. Through a series of transcriptomic, *in*

246   *vitro*, and *in vivo* analyses, we identified TIAM1 expression in pericytes as a morphologic

247   regulator that maintains tissue specificity within the adipose niche.

248

249   Pericytes located in the basement membrane are in contact with the endothelium of

250   capillaries, and as such, are strongly influenced by a variety of physical stimuli such as

251   fluid stress compression and microenvironmental tension (21). Studies have shown that

252   changes in the differentiation potential of mesenchymal progenitor cells are dependent

253   on tissue stiffness *in vitro* (22, 23). For example, progenitor cells cultured on gels

254   demonstrate heightened chondrogenic and adipogenic differentiation potential compared

255   to those cultured on stiff surfaces (22), and the use of supramolecular hydrogels at

256   different stiffnesses determine neuronal, osteogenic, and chondrogenic differentiation

257   (24). TIAM1 is a Rac1specific guanine nucleotide exchange factor and negatively

258   regulates RhoA/ROCK pathways. Rac1 and RhoA/ROCK are two reciprocal signaling

259   pathways regulate cell migration and proliferation through actin organization (25). Rac1

260   activation has been shown to induce membrane ruffles and lamellipodia in fibroblasts. In

261   contrast, RhoA/ROCK has been suggested to increase differentiation in myogenesis and

262   decrease adipogenesis via modulation of cytoskeletal tension and organization in

263   pluripotent stem cells and fibroblasts (26). These results in cytoskeletal arrangements

264   that ultimately affect migration, proliferation, and adhesion (27-29). In the context of

265   differentiation, prior reports have shown that high RhoA/ROCK activity is associated with

266   osteogenic differentiation (26, 30), while a loss of RhoA and activation of Rac1 leads to

267   an adipogenic phenotype (26, 31, 32). In this study, we confirmed these observations and

268   further expanded the role that TIAM1 plays in modulating these signaling pathways to

269   regulate cell morphology and ultimately, cellular differentiation in pericytes. Cytoskeleton-

270   dependent signaling pathways in pericytes regulate physical and chemical

271   interconnections in the actin network, as well in the extracellular matrix (33). Actin

272   assembly modifications play crucial roles in pericyte shape and contractility (33, 34). In

273   the context of tissue specificity, the interplay of microenvironmental clues such, as

274   extracellular matrix stiffness, may help determine cell phenotype and influence

275   differentiation potential (35, 36). TIAM1 regulates the RhoA/ROCK family through the

276   RhoA/ROCK inhibitor, Rac1 and serve as a novel regulator of tissue specificity pericytes

277   between adipose tissue and bone. These reciprocal pathways may aid in changing MSC

278   shape which in turn can regulate the degree of osteogenic or adipogenic differentiation.

279   The extent to which TIAM1 directly regulates adipogenesis, and/or indirectly regulates

280   adipogenesis through Rac1 or in combination with other Rac associated pathways

281   remains in question.

282

283   Important limitations exist in the study. Although TIAM1 is enriched in undifferentiated

284   adipose-derived pericytes, as shown in our transcriptomic analyses, it is a curious finding

285   that while TIAM1 remains unchanged during in vitro adipogenesis, its misexpression

286   resulted in significant changes in the degree of adipogenic differentiation. Future studies

287   could pursue in depth how TIAM1 directly or indirectly regulates adipogenesis. As a

288   second limitation, the present study is only shown in adipose-derived CD146+ pericytes

289   and has not been tested in other mesenchymal stem cell types. In future studies, global

290   or tissue-specific TIAM1 knockout mice may be better to elucidate the role of TIAM1 in

291   pericyte differentiation decisions.

292

293   In conclusion, TIAM1 is a key regulator of cytoskeletal dynamics, affecting adipose-

294   derived pericyte morphology and differentiation potential toward adipocytic versus

295   osteoblastic fates. Studies on TIAM1 misexpression suggest a role for TIAM1 in tissue-

296   specific pericyte differentiation decisions by regulating cytoskeletal morphology through

297   Rac1 and RhoA/ROCK signaling pathways. This was confirmed in xenograft animal

298   models. Further study of TIAM1-Rac1 and RhoA/ROCK regulation of other tissue specific

299   mesenchymal precursor cell fates, and by extension development of new strategies for

300   tissue engineering, will be worth future investigation.

301

302   **Materials and Methods**

303   **Isolation and culture of periosteal or adipose CD146$^+$ pericytes**

304   CD146$^+$ pericytes were isolated from human adipose tissue and periosteum via

305   fluorescence-activated cell sorting (FACS) (4, 37, 38). Total of N=3 adipose and N=3

306   periosteum samples were obtained from adult patient donors. Pericytes from 6 individual

307   patients were collected for microarray, and in vitro, in vivo assays.

308   N=3 adipose samples from three different patient sources were analyzed and collected

309   by flow cytometry by the method described in a previous study (39, 40) (summary of

310   antibodies presented in **Supplementary Table S1**). Briefly, passage 3 expanded

311   CD146+ pericytes were analyzed by FlowJo software. In this manner, the FACS-purified

312   CD146^{+} pericytes were snap frozen for RNA isolation, culture expanded to passage 3-8

313   for *in vitro* studies, or applied in a mouse intramuscular implantation model. For *in vitro*

314   expansion, all cells were cultured in non-clonal monolayer at 37°C in a humidified

315   atmosphere containing 95% air and 5% CO_2. FACS-purified CD146^{+} pericytes were

316   cultured in DMEM medium with 10% fetal bovine serum (FBS) (Gibco, Grand island, NY,

317   USA) and 1% penicillin/streptomycin (Life technologies corporation, Gaithersburg, MD,

318   USA). The medium was changed every 3 days, unless otherwise noted. Pericytes at

319   passages 3 to 8 were used for *in vitro* and *in vivo* assays. Rac activity was inhibited using

320   NSC23766 (Selleckchem, Houston, TX, USA), reconstituted in sterile water, and used at

321   a final concentration of 5 µM. ROCK signaling was inhibited using Y-27632 (Selleckchem,

322   Houston, TX, USA), reconstituted in dimethyl sulfoxide (DMSO), and used at a final

323   concentration of 10 µM. NSC23766 or Y27632 were added at the time of cell seeding.

324   For inhibitor studies, a DMSO vehicle control was present in all treatment groups.

325   **Microarray analysis**

326

327   The transcriptomes of N=6 CD146^{+} periosteal and adipose pericytes from total of six

328   different patients were examined by microarray (N=3 periosteal and N=3 adipose

329   sources). Briefly, total RNA was extracted from passage 3 CD146^{+} pericytes by Trizol

330   (Life technologies corporation). After purification, the RNA samples were sent to the JHMI

331   Transcriptomics and Deep Sequencing Core (JHU, Baltimore, MD, USA) for analysis

332   using an Affymetrix Clariom D microarray (Affymetrix, Santa Clara, CA, USA). Microarray

333   data was obtained from the Gene Expression Omnibus (GEO) repository (accession

334   number GSE125545). Data analyses were performed using software packages including

335 Partek Genomics Suite, Spotfire DecisionSite with Functional Genomics, and QIAGEN

336 Ingenuity® Pathway Analysis.

337

338 **Immunohistochemistry and microscopy**

339 For histology, three healthy human subcutaneous fat tissue samples were identified in

340 our surgical pathology archives (Johns Hopkins University). Samples were obtained

341 under IRB approval with a waiver of informed consent. Human fat tissues were embedded

342 in optimal cutting temperature compound (OCT) (Sakura, Torrance, CA) and

343 cryosectioned at 20 µm thicknesses for immunofluorescent staining by methods

344 described in the previous paper (Antibodies used are listed in **Supplemental Table S1**)

345 (4, 41). A Zeiss 800 confocal microscope (Zeiss, Thornwood, NY) was used for imaging

346 immunofluorescent staining or a Leica DM6 B microscope (Leica Microsystems Inc,

347 Wetzlar, Germany) was used for imaging immunohistochemical staining.

348

349 **Small interfering RNA (siRNA) and transfection**

350 Knockdown of *TIAM1* in CD146+ adipose pericytes were performed using Silencer Select

351 chemically synthesized siRNA (Thermo Fisher Scientific, Cat# 439824; S14138).

352 Pericytes at passage 3-8 were seeded in 12-well plates at a density of 5×10^4 cells per

353 well. At 50% confluence, basal medium was replaced with antibiotic-free basal medium.

354 Transfection was performed using X-tremeGENE siRNA Transfection Reagent (Sigma-

355 Aldrich) and 150 pM *TIAM1-1* siRNA or scramble siRNA diluted in minimal essential

356 medium (Opti-MEM) (42). To confirm siRNA efficiency, at 2 h post-transfection, the

357 medium was replaced with basal medium, and the efficiency of the knockdown was

358 validated using qRT-PCR and immunocytochemistry (ICC).

359 **Plasmid transfected overexpression**

360 *TIAM1* overexpression was assayed using a human *TIAM1* open reading frame (ORF)

361 mammalian expression plasmid (RG220233, Origene, Rockville, MD). 24 h prior to

362 transfection, CD146$^+$ adipose pericytes at passage 3-8 were seeded in 12-well plates at

363 a density of 5×10^4 cells per well. For transfection were performed at 60% confluence,

364 1 μg of TIAM1 plasmid or control plasmid was mixed with 3 μl of Roche Xtreme gene HP

365 transfection reagent in 100 μL of Opti-MEM and incubated at RT for 30 min. The

366 DNA/Transfection reagent mixture was then added in drops to wells (42). qRT-PCR and

367 ICC were used to measure *TIAM1* gene expression and to confirm the efficacy of the

368 plasmid.

369 **Osteogenic differentiation assays**

370 CD146$^+$ adipose pericytes from 3 to 8 passages were seeded in 12-well plates at a

371 density of 5×10^5 cells per well. Osteogenic differentiation medium (ODM) consisted of

372 DMEM, 10% FBS, 1% penicillin/streptomycin with 10 mmol·L^{-1} β-glycerophosphate,

373 50 μmol·L^{-1} ascorbic acid, and 1 mmol·L^{-1} dexamethasone. 24 h after cell seeding, basal

374 medium was replaced with ODM and replenished every 3 days.

375 For ALP and Alizarin Red (AR) staining, cells were washed with PBS and fixed with 4%

376 formaldehyde from 7 to 10 days of differentiation. Next, cells were stained with diazonium

377 salt with 4% napthol AS-MX phosphate alkaline solution in RT for 15 min for alkaline

378 phosphatase detection and with 2% AR solution at RT for 10 min for bone nodule

379 deposition (4, 40, 42-44). Pictures were taken using an Olympus Epson scanner (Los

380 Angeles, CA, USA). For quantification, bone nodules were dissolved in 0.1 N sodium

381 hydroxide and quantified using an Epoch microspectrophotometer (BioTek, Winooski, VT,

382 USA) by an absorbance at 548 nm. All experiments were performed with $n = 3$ human

383 samples per anatomic depot and in triplicate wells (biologic and technical triplicate).

384

385 **Adipogenic differentiation assays**

386 CD146$^+$ adipose pericytes from 3 to 8 passages were seeded in 12-well plates at a

387 density of 2×10^5 cells per well and allowed to adhere overnight. 24 h after seeding, the

388 basal medium was replaced with adipogenic differentiation medium and replenished

389 every 3 days (Mesencult Adipogenic Differentiation medium, StemCell technologies Inc.,

390 Vancouver, BC). Oil red O staining was performed after 10 d of differentiation (4, 40, 42).

391 Cells were washed with PBS and fixed with 4% PFA for 15 min. After fixation, cells were

392 washed with water and 500 µL of Oil red O staining solution. Oil red O stock solution was

393 prepared by dissolving 0.5 g of Oil red O in 100 mL isopropanol. Oil red O staining solution

394 was prepared by dilution of a stock solution with distilled water in a 3:2 ratio, followed by

395 filtration. Oil red O staining was performed for 30 min at 37°C. Following incubation, cells

396 were washed with tap water, followed by microscopy. After imaging, Oil Red O stain was

397 extracted with 100% isopropanol for 5 min followed by an absorbance at 548 nm for

398 quantification. All experiments were performed with $n = 3$ human samples per anatomic

399 depot and in triplicate wells (biologic and technical triplicate).

400

Proliferation assays

Proliferation assays were performed in 96-well plates (2 × 103 cells/well) and measured for up to 72 h using the CellTiter96 AQueous One Solution Cell Proliferation Assay kit (MTS, G358A; Promega, Madison, WI) (44). Briefly, 20 μL of MTS solution was added to each well and incubated for 1 h at 37°C. The absorbance was assayed at 490 nm using an Epoch microspectrophotometer (Bio-Tek, Winooski, VT).

Quantitative (q)RT-PCR

Specific gene expression among CD146^{+} adipose pericytes were assayed by qRT-PCR at 0, 3, and 7 d of osteogenic/adipogenic differentiation, adapted from prior methods (38, 42, 44). The frequency of CD146+CD31-CD45- pericytes by anatomic depot of origin and percentage of CD146+CD31-CD45- of total FACS events was reported in the previous study (4). Total RNA was extracted using TRIzol Reagent (Life technologies corporation). In total, 1 μg of total RNA from each sample was subjected to first-strand complementary deoxyribonucleic acid (cDNA) synthesis using the iScript™ cDNA Synthesis Kit (Bio-Rad) to a final volume of 20 μL. The reverse transcription reaction was performed at 25°C for 5 min, followed by 46°C for 20 min and 95°C for 1 min. For qRT-PCR, the reaction was performed using 2× SYBR green RT-PCR master mix and a QuantStudio 5 Real-Time PCR system instrument (Thermo Scientific, Waltham, MA). qRT-PCR was performed using 384-well optical plates at 95°C for 10 min, followed by 40 cycles at 95°C for 15 s and at 60°C for 60 s. The relative quantification of gene expression was performed using a threshold cycle (CT) method according to the manufacturer's protocol and was normalized to the expression levels of the housekeeping gene *glyceraldehyde 3-*

424 *phosphate dehydrogenase* (*GAPDH*) in each sample. Primer sequences are shown in

425 **Supplementary Table S3**.

426

427 **Cell morphology**

428 Pericytes were seeded in 1 x 10^5 per mL to visualize single cell populations. After culturing

429 cells for 48 h, cells were fixed with 4% PFA and incubated with a TIAM1 primary antibody

430 overnight. This was followed by staining with the secondary antibody and Oregon green

431 488 phalloidin (Thermo Fisher, Waltham, MA, USA) for 30 mins at RT. Afterwards,

432 mounting medium with DAPI was applied before covering the chamber slide with glass

433 coverslips. Images of the stained pericytes were captured and analyzed using a Zeiss

434 LSM 800 Confocal Microscope. The intensity of TIAM1 immunostaining was evaluated as

435 mean fluorescence intensity across five different random microscopic areas at 63X

436 magnification. Cellular morphology, including width and length of individual cells from five

437 different random microscopic areas at 63X magnification, was calculated using ImageJ

438 software (ImageJ 1.47v, NIH, Thornwood, Bethesda, MD, USA).

439

440 **Intramuscular implantation**

441 Animals were housed and experiments were performed in accordance with institutional

442 guidelines at the Johns Hopkins University. All animal experiments were performed

443 according to Johns Hopkins University Animal Care and Use Committee (ACUC)

444 approved protocols (MO19M266). A demineralized bone matrix (DBM) Putty (DBX,

445 courtesy of Musculoskeletal Transplant Foundation, Edison, NJ) was used for the ectopic

446 bone formation assay in mice. Briefly, human CD146$^+$ adipose pericytes were pre-treated

447 with siRNA for knockdown or plasmid for overexpression 48 h before implantation. The

448 scramble siRNA and control plasmid were served as control compared to the TIAM1

449 siRNA knockdown and TIAM1 plasmid overexpression. Cells were resuspended at a

450 density of 7.5 ×10^7 cells per mL in PBS. For each implantation sample, 40 µL of cell

451 suspension was mixed mechanically with 50 mg of DBX allograft putty (3 million total cells

452 in 40 µL PBS) and implanted intramuscularly into the thigh muscle pouch of 10-week-old

453 male athymic mice weight 28~33g (The Jackson Laboratory, Bar Harbor, Maine, USA). A

454 single implant was placed per mouse. N=4 mice per treatment group, for a total of 16

455 mice were used in the experiment. Briefly, animals were anesthetized by isoflurane

456 inhalation and premedicated with buprenorphine. Incisions in the bilateral hindlimbs were

457 made, and pockets were cut in the biceps femoris muscles parallel to the muscle fiber

458 long axis by blunt dissection (45). Dissection methods and the surgical manipulation of

459 tissues were kept as constant as possible across animals. After implantation of the

460 cell + scaffold composite, the fascia overlying the muscle was sutured with a simple

461 continuous pattern, and the skin was closed in a separate layer using 5-0 Vicryl (Ethicon,

462 San Angelo, TX).

463

464 **MicroCT imaging and analysis**

465 Tissues were harvested 8 weeks after implantation and fixed in 4% PFA for 24 h,

466 transferred to PBS, and scanned using high-resolution microcomputed tomography

467 (microCT) (SkyScan 1275; Bruker MicroCT N.V) at an image resolution of 15 µm with the

468 following settings: aluminum filter of 1 mm, X-ray voltage of 65 kVP, anode current of

469 153 µA, exposure time of 160–218 ms, frame average of 6, and rotation step of 0.3

470 degrees (4). Three-dimensional images were then reconstructed from the 2D X-ray

471 projections by implementing the Feldkamp algorithm using a commercial NRecon

472 software package (2.0.4.0 SkyScan). For the 3D morphometric analyses of images,

473 CTVox and CTAn softwares (1.13 SkyScan) were used. Volumes of interest were shaped

474 by polygons to cover the new bone around the femur with a threshold of 65. The amount

475 of bone formation was analyzed and quantified.

476

477 **Statistical analysis**

478 Statistical analyses were performed in GraphPad Software 6.0. Quantitative data is

479 expressed as mean ± 1 SD. All data were normally distributed. A Student's t test was

480 used for two-group comparisons, and one-way ANOVA test was used for comparisons of

481 three or more groups, followed by Tukey's post hoc test.

482

483 **Study Approval**

484 All animal procedures were approved by IACUC of the Johns Hopkins University (JHU).

485 Human samples were obtained under approval from the JHU, IRB with a waiver of

486 informed consent.

487

488 **Authors' Contribution**

489 G.C.H., A.Z.L., M.A.G.S.: Collection and assembly of data, data analysis and

490 interpretation, and manuscript writing. Y.W., A.Z.L., D.L., S.N., K.B., C.M., J.X., S.W.,

491 B.P., C.M.: Collection and assembly of data. A.W.J: Provision of study material,

conception, and design, financial support, manuscript writing, and final approval of manuscript.

Conflicts of interest

Research unrelated to the work presented herein was supported in the James laboratory by Musculoskeletal Transplant Foundation (MTF) Biologics and Novadip Biosciences. A.W.J. is a paid consultant for Novadip and Lifesprout. This arrangement has been reviewed and approved by the Johns Hopkins University in accordance with its conflict of interest policies. The authors have declared that no further conflict of interest exists.

<div style="text-align: center;">References</div>

514
515
516 1. Lojewski X, Srimasorn S, Rauh J, Francke S, Wobus M, Taylor V, et al. Perivascular
517   Mesenchymal Stem Cells From the Adult Human Brain Harbor No Instrinsic
518   Neuroectodermal but High Mesodermal Differentiation Potential. *Stem Cells Transl*
519   *Med.* 2015;4(10):1223-33.
520 2. Mierzejewski B, Grabowska I, Jackowski D, Irhashava A, Michalska Z, Streminska W,
521   et al. Mouse CD146+ muscle interstitial progenitor cells differ from satellite cells
522   and present myogenic potential. *Stem Cell Res Ther.* 2020;11(1):341.
523 3. Murray IR, West CC, Hardy WR, James AW, Park TS, Nguyen A, et al. Natural history
524   of mesenchymal stem cells, from vessel walls to culture vessels. *Cell Mol Life Sci.*
525   2014;71(8):1353-74.
526 4. Xu J, Li D, Hsu CY, Tian Y, Zhang L, Wang Y, et al. Comparison of skeletal and soft
527   tissue pericytes identifies CXCR4(+) bone forming mural cells in human tissues.
528   *Bone Res.* 2020;8:22.
529 5. Pierantozzi E, Vezzani B, Badin M, Curina C, Severi FM, Petraglia F, et al. Tissue-
530   Specific Cultured Human Pericytes: Perivascular Cells from Smooth Muscle Tissue
531   Have Restricted Mesodermal Differentiation Ability. *Stem Cells Dev.* 2016;25(9):674-
532   86.
533 6. Sacchetti B, Funari A, Remoli C, Giannicola G, Kogler G, Liedtke S, et al. No Identical
534   "Mesenchymal Stem Cells" at Different Times and Sites: Human Committed
535   Progenitors of Distinct Origin and Differentiation Potential Are Incorporated as
536   Adventitial Cells in Microvessels. *Stem Cell Reports.* 2016;6(6):897-913.
537 7. Hindle P, Khan N, Biant L, and Peault B. The Infrapatellar Fat Pad as a Source of
538   Perivascular Stem Cells with Increased Chondrogenic Potential for Regenerative
539   Medicine. *Stem Cells Transl Med.* 2017;6(1):77-87.
540 8. James AW, and Peault B. Perivascular Mesenchymal Progenitors for Bone
541   Regeneration. *J Orthop Res.* 2019;37(6):1221-8.
542 9. Malliri A, van der Kammen RA, Clark K, van der Valk M, Michiels F, and Collard JG.
543   Mice deficient in the Rac activator Tiam1 are resistant to Ras-induced skin tumours.
544   *Nature.* 2002;417(6891):867-71.
545 10. Hofbauer SW, Krenn PW, Ganghammer S, Asslaber D, Pichler U, Oberascher K, et al.
546   Tiam1/Rac1 signals contribute to the proliferation and chemoresistance, but not
547   motility, of chronic lymphocytic leukemia cells. *Blood.* 2014;123(14):2181-8.
548 11. Minard ME, Ellis LM, and Gallick GE. Tiam1 regulates cell adhesion, migration and
549   apoptosis in colon tumor cells. *Clin Exp Metastasis.* 2006;23(5-6):301-13.
550 12. Wang YK, and Chen CS. Cell adhesion and mechanical stimulation in the regulation
551   of mesenchymal stem cell differentiation. *J Cell Mol Med.* 2013;17(7):823-32.
552 13. Yeo GC, and Weiss AS. Soluble matrix protein is a potent modulator of mesenchymal
553   stem cell performance. *Proc Natl Acad Sci U S A.* 2019;116(6):2042-51.
554 14. Habets GG, Scholtes EH, Zuydgeest D, van der Kammen RA, Stam JC, Berns A, et al.
555   Identification of an invasion-inducing gene, Tiam-1, that encodes a protein with
556   homology to GDP-GTP exchangers for Rho-like proteins. *Cell.* 1994;77(4):537-49.
557 15. Malliri A, van Es S, Huveneers S, and Collard JG. The Rac exchange factor Tiam1 is
558   required for the establishment and maintenance of cadherin-based adhesions. *J Biol*
559   *Chem.* 2004;279(29):30092-8.

560   16.   Mertens AE, Rygiel TP, Olivo C, van der Kammen R, and Collard JG. The Rac activator
561   Tiam1 controls tight junction biogenesis in keratinocytes through binding to and
562   activation of the Par polarity complex. *J Cell Biol.* 2005;170(7):1029-37.
563   17.   Michiels F, Habets GG, Stam JC, van der Kammen RA, and Collard JG. A role for Rac in
564   Tiam1-induced membrane ruffling and invasion. *Nature.* 1995;375(6529):338-40.
565   18.   Sander EE, van Delft S, ten Klooster JP, Reid T, van der Kammen RA, Michiels F, et al.
566   Matrix-dependent Tiam1/Rac signaling in epithelial cells promotes either cell-cell
567   adhesion or cell migration and is regulated by phosphatidylinositol 3-kinase. *J Cell*
568   *Biol.* 1998;143(5):1385-98.
569   19.   Boissier P, and Huynh-Do U. The guanine nucleotide exchange factor Tiam1: a Janus-
570   faced molecule in cellular signaling. *Cell Signal.* 2014;26(3):483-91.
571   20.   Guo X, Wang M, Jiang J, Xie C, Peng F, Li X, et al. Balanced Tiam1-rac1 and RhoA
572   drives proliferation and invasion of pancreatic cancer cells. *Mol Cancer Res.*
573   2013;11(3):230-9.
574   21.   Spindler V, Schlegel N, and Waschke J. Role of GTPases in control of microvascular
575   permeability. *Cardiovasc Res.* 2010;87(2):243-53.
576   22.   Park JS, Chu JS, Tsou AD, Diop R, Tang Z, Wang A, et al. The effect of matrix stiffness
577   on the differentiation of mesenchymal stem cells in response to TGF-beta.
578   *Biomaterials.* 2011;32(16):3921-30.
579   23.   Pek YS, Wan AC, and Ying JY. The effect of matrix stiffness on mesenchymal stem cell
580   differentiation in a 3D thixotropic gel. *Biomaterials.* 2010;31(3):385-91.
581   24.   Yourek G, Hussain MA, and Mao JJ. Cytoskeletal changes of mesenchymal stem cells
582   during differentiation. *ASAIO J.* 2007;53(2):219-28.
583   25.   Gao Y, Dickerson JB, Guo F, Zheng J, and Zheng Y. Rational design and
584   characterization of a Rac GTPase-specific small molecule inhibitor. *Proc Natl Acad*
585   *Sci U S A.* 2004;101(20):7618-23.
586   26.   McBeath R, Pirone DM, Nelson CM, Bhadriraju K, and Chen CS. Cell shape,
587   cytoskeletal tension, and RhoA regulate stem cell lineage commitment. *Dev Cell.*
588   2004;6(4):483-95.
589   27.   Chauhan BK, Lou M, Zheng Y, and Lang RA. Balanced Rac1 and RhoA activities
590   regulate cell shape and drive invagination morphogenesis in epithelia. *Proc Natl*
591   *Acad Sci U S A.* 2011;108(45):18289-94.
592   28.   Goldberg L, and Kloog Y. A Ras inhibitor tilts the balance between Rac and Rho and
593   blocks phosphatidylinositol 3-kinase-dependent glioblastoma cell migration. *Cancer*
594   *Res.* 2006;66(24):11709-17.
595   29.   Nayak RC, Chang KH, Vaitinadin NS, and Cancelas JA. Rho GTPases control specific
596   cytoskeleton-dependent functions of hematopoietic stem cells. *Immunol Rev.*
597   2013;256(1):255-68.
598   30.   Calzado-Martin A, Mendez-Vilas A, Multigner M, Saldana L, Gonzalez-Carrasco JL,
599   Gonzalez-Martin ML, et al. On the role of RhoA/ROCK signaling in contact guidance
600   of bone-forming cells on anisotropic Ti6Al4V surfaces. *Acta Biomater.*
601   2011;7(4):1890-901.
602   31.   Das RK, Zouani OF, Labrugere C, Oda R, and Durrieu MC. Influence of nanohelical
603   shape and periodicity on stem cell fate. *ACS Nano.* 2013;7(4):3351-61.

604   32.   Kunitomi H, Oki Y, Onishi N, Kano K, Banno K, Aoki D, et al. The insulin-PI3K-Rac1
605   axis contributes to terminal adipocyte differentiation through regulation of actin
606   cytoskeleton dynamics. *Genes Cells.* 2020;25(3):165-74.
607   33.   Kutcher ME, Kolyada AY, Surks HK, and Herman IM. Pericyte Rho GTPase mediates
608   both pericyte contractile phenotype and capillary endothelial growth state. *Am J*
609   *Pathol.* 2007;171(2):693-701.
610   34.   Lee S, Zeiger A, Maloney JM, Kotecki M, Van Vliet KJ, and Herman IM. Pericyte
611   actomyosin-mediated contraction at the cell-material interface can modulate the
612   microvascular niche. *J Phys Condens Matter.* 2010;22(19):194115.
613   35.   Isomursu A, Lerche M, Taskinen ME, Ivaska J, and Peuhu E. Integrin signaling and
614   mechanotransduction in regulation of somatic stem cells. *Exp Cell Res.*
615   2019;378(2):217-25.
616   36.   Engler AJ, Sen S, Sweeney HL, and Discher DE. Matrix elasticity directs stem cell
617   lineage specification. *Cell.* 2006;126(4):677-89.
618   37.   Meyers CA, Wang C, Xu J, Pan HC, Shen J, Ting K, et al. Assessing the Bone-Forming
619   Potential of Pericytes. *Methods Mol Biol.* 2021;2235:127-37.
620   38.   Wang Y, Xu J, Chang L, Meyers CA, Zhang L, Broderick K, et al. Relative contributions
621   of adipose-resident CD146(+) pericytes and CD34(+) adventitial progenitor cells in
622   bone tissue engineering. *NPJ Regen Med.* 2019;4:1.
623   39.   Xu J, Li D, Hsu CY, Tian Y, Zhang L, Wang Y, et al. Comparison of skeletal and soft
624   tissue pericytes identifies CXCR4(+) bone forming mural cells in human tissues.
625   *Bone Res.* 2020;8(1):22.
626   40.   Xu J, Wang Y, Hsu CY, Negri S, Tower RJ, Gao Y, et al. Lysosomal protein surface
627   expression discriminates fat- from bone-forming human mesenchymal precursor
628   cells. *Elife.* 2020;9.
629   41.   Wang Y, Xu J, Meyers CA, Gao Y, Tian Y, Broderick K, et al. PDGFRalpha marks
630   distinct perivascular populations with different osteogenic potential within adipose
631   tissue. *Stem Cells.* 2020;38(2):276-90.
632   42.   Meyers CA, Xu J, Asatrian G, Ding C, Shen J, Broderick K, et al. WISP-1 drives bone
633   formation at the expense of fat formation in human perivascular stem cells. *Sci Rep.*
634   2018;8(1):15618.
635   43.   Wang Y, Negri S, Li Z, Xu J, Hsu CY, Peault B, et al. Anti-DKK1 Enhances the Early
636   Osteogenic Differentiation of Human Adipose-Derived Stem/Stromal Cells. *Stem*
637   *Cells Dev.* 2020;29(15):1007-15.
638   44.   Xu J, Wang Y, Hsu CY, Gao Y, Meyers CA, Chang L, et al. Human perivascular stem
639   cell-derived extracellular vesicles mediate bone repair. *Elife.* 2019;8.
640   45.   Asatrian G, Chang L, and James AW. Muscle pouch implantation: an ectopic bone
641   formation model. *Methods Mol Biol.* 2014;1213:185-91.
642

643

644

645

646 **Graphic Abstract**
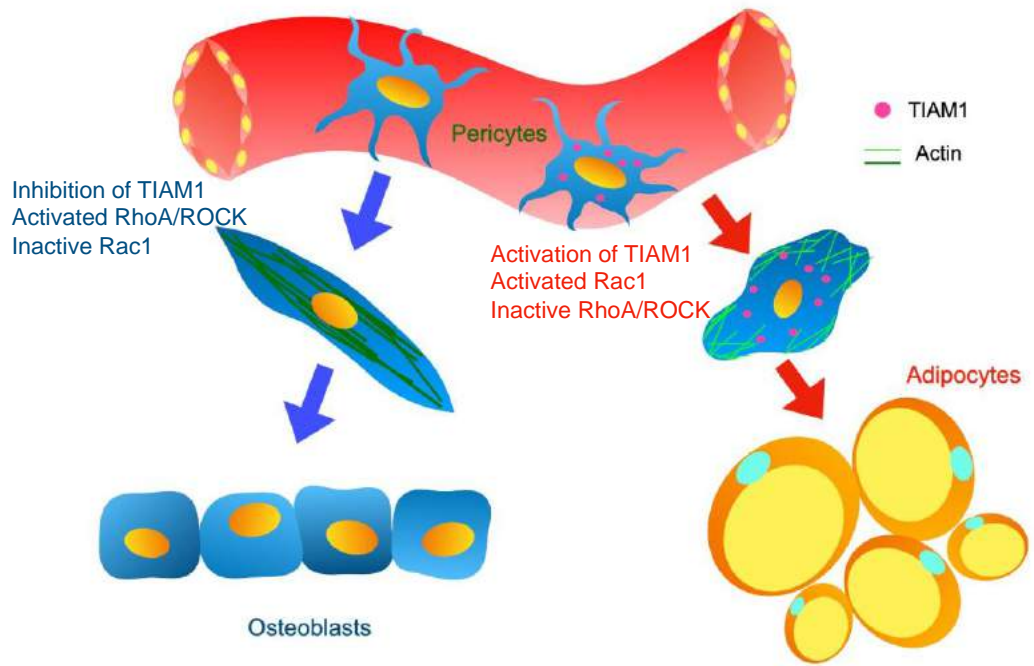
647

648

649

650

651
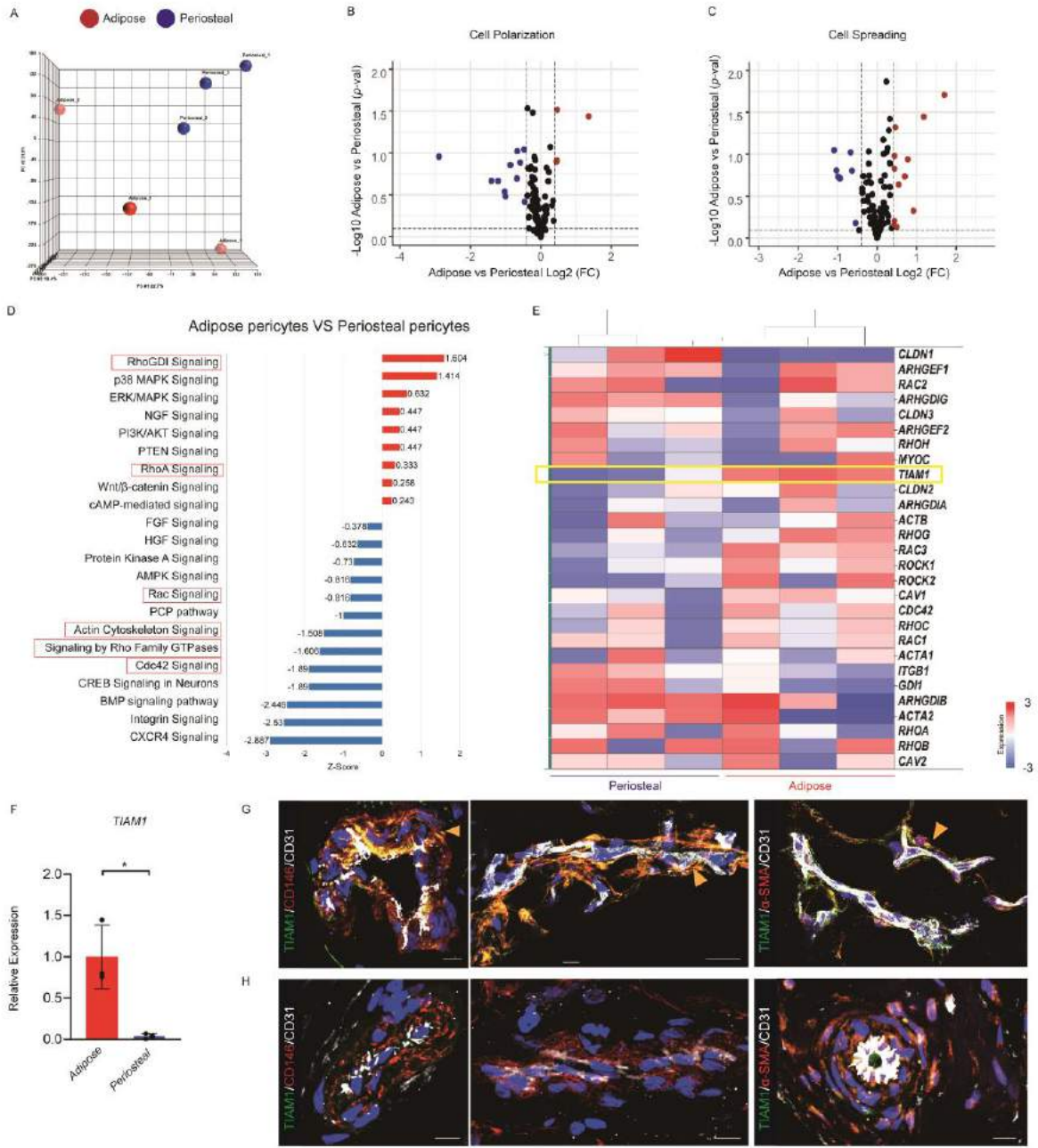
652

653

654

655

656

657

658

659

Figure 1.

666 **Figure 1. TIAM1 is highly expressed in human pericytes within adipose tissue but**

667 **not skeletal tissue. (A-E)** Transcriptome of skeletal (periosteal) and adipose

668 CD146⁺ pericytes, by Clariom D microarray among undifferentiated, culture-expanded

669 cells of equal passage. **(A)** Principal component analysis among periosteal and adipose

670 CD146⁺ pericytes. Each dot represents pericytes from different patients. **(B,C)** Volcano

671 plots involving genes associated with cell polarization (B) and cell spreading (C) among

672 adipose and periosteal pericytes. Red dots indicate transcripts enriched in adipose

673 pericytes, whereas blue dots indicate transcripts enriched in periosteal pericytes. **(D)**

674 Ingenuity Pathway Analysis (IPA) demonstrating differentially activated pathways among

675 adipose versus periosteal CD146⁺ pericytes. Red boxes indicate pathways of interest in

676 cytoskeletal organization. **(E)** Heatmap of genes associated with Rho GTPases, including

677 *TIAM1*. **(F)** Validation of differential *TIAM1* expression among CD146⁺ pericytes from

678 adipose and periosteal sources, by quantitative RT-PCR. **(G)** Immunofluorescent staining

679 of TIAM1 in microvessels of subcutaneous human adipose tissue. Co-immunostaining for

680 pericyte markers (CD146 and α-SMA) and CD31 performed. **(H)** Immunofluorescent

681 staining of TIAM1 in microvessels of human periosteum. Co-immunostaining for pericyte

682 markers (CD146 and a-SMA) and CD31 performed. Yellow arrow indicates co-localization

683 of CD146 or α-SMA (Red) and TIAM1 (Green) immunoreactivity. Endothelium (CD31)

684 appear white. Nuclear counterstain appears blue. Scale bars: 10 μm. *P<0.05.

685 Statistical analysis was performed using a two-sample Student's t-test.

686

687

688

689   **Figure 2.**

690

691

692

693

694
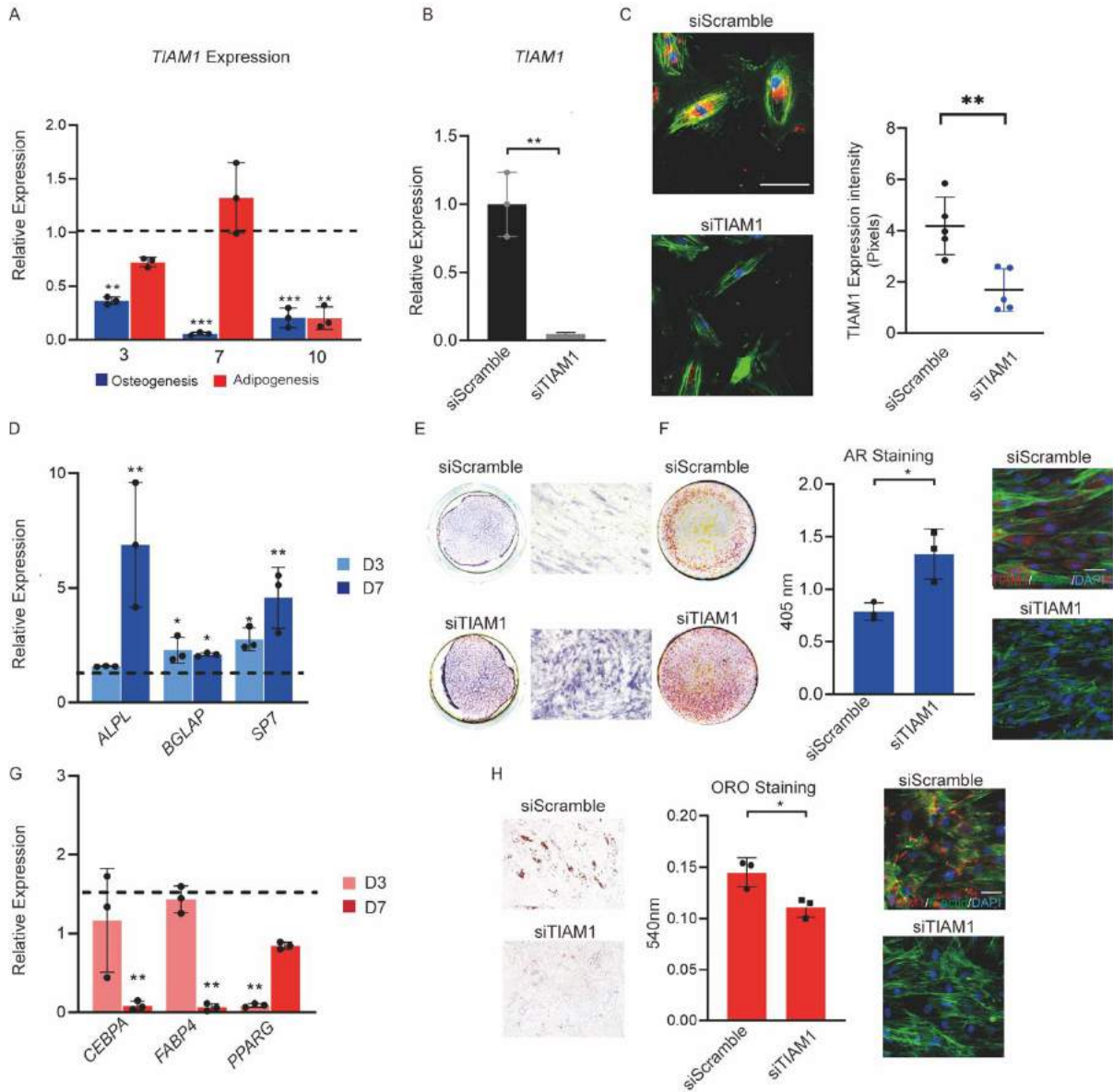
Figure 2. *TIAM1* **knockdown favors osteogenic over adipogenic differentiation of human adipose tissue-derived CD146⁺ pericytes.** Human pericytes from dissociated subcutaneous white adipose tissue were FACS isolated as a CD146$^+$CD34$^-$CD45$^-$CD31$^-$ cell population and cultured under osteogenic or adipogenic differentiation conditions. **(A)** *TIAM1* expression during osteogenic and adipogenic differentiation of human pericytes, as assessed by qRT-PCR. Dashed lines indicate expression among undifferentiated cells. **(B)** Knockdown (KD) efficiency by qRT-PCR 48 hrs after treatment with *TIAM1* siRNA or scramble siRNA. **(C)** Knockdown efficiency by fluorescent immunocytochemistry for TIAM1 and semi-quantitative analysis 48 hrs after KD. TIAM1 immunostaining appears red, while F-actin staining appears green. Random images (N=5) of fluorescent staining were obtained for semiquantitation of TIAM1 (Red) or F-actin (Green) area (mean Red or Green fluorescent area per field view). **(D)** Osteogenic gene markers at d 3 and 7 of osteogenic differentiation among *TIAM1* KD pericytes, assessed by qRT-PCR. Dashed lines indicate expression among scramble siRNA at the same timepoint. *ALPL: Alkaline Phosphatase; BGLAP: Osteocalcin; SP7: Osterix.* **(E)** Alkaline phosphatase (ALP) staining shown by whole well and representative 10x microscopical images, d 7 of differentiation. **(F)** Alizarin Red staining with quantification on d 10 of osteogenic differentiation, shown by whole well images. Immunohistochemistry showed the TIAM1 and F-actin expression during osteogenesis **(G)** Adipogenic gene marker expression at d 3 and 7 of adipogenic differentiation among *TIAM1* KD pericytes, assessed by qRT-PCR. Dashed lines indicate expression among scramble siRNA at the same timepoint. *CEBPA: CCAAT Enhancer Binding Protein Alpha; FABP4: fatty acid-binding protein 4; PPARG: peroxisome proliferator-activated receptor.* **(H)** Oil red O

718 staining and quantification, d 10 of adipogenic differentiation (representative 10x

719 magnification images shown). Immunohistochemistry showed the TIAM1 and F-actin

720 expression during adipgenesis. *$P<0.05$; **$P<0.01$ in comparison to scramble siRNA at

721 the corresponding timepoint. Experiments performed in at least triplicate experimental

722 replicates. Statistical analysis was performed using a two-sample Student's t-test or One-

723 way ANOVA test was used for comparisons of three or more groups, followed by Tukey's

724 post hoc test. White scale bars: 20 µm.

725

726

727

728

729

730

731

732

733

734

735

736

737

738

739

740

741   **Figure 3.**

742

743

744

745
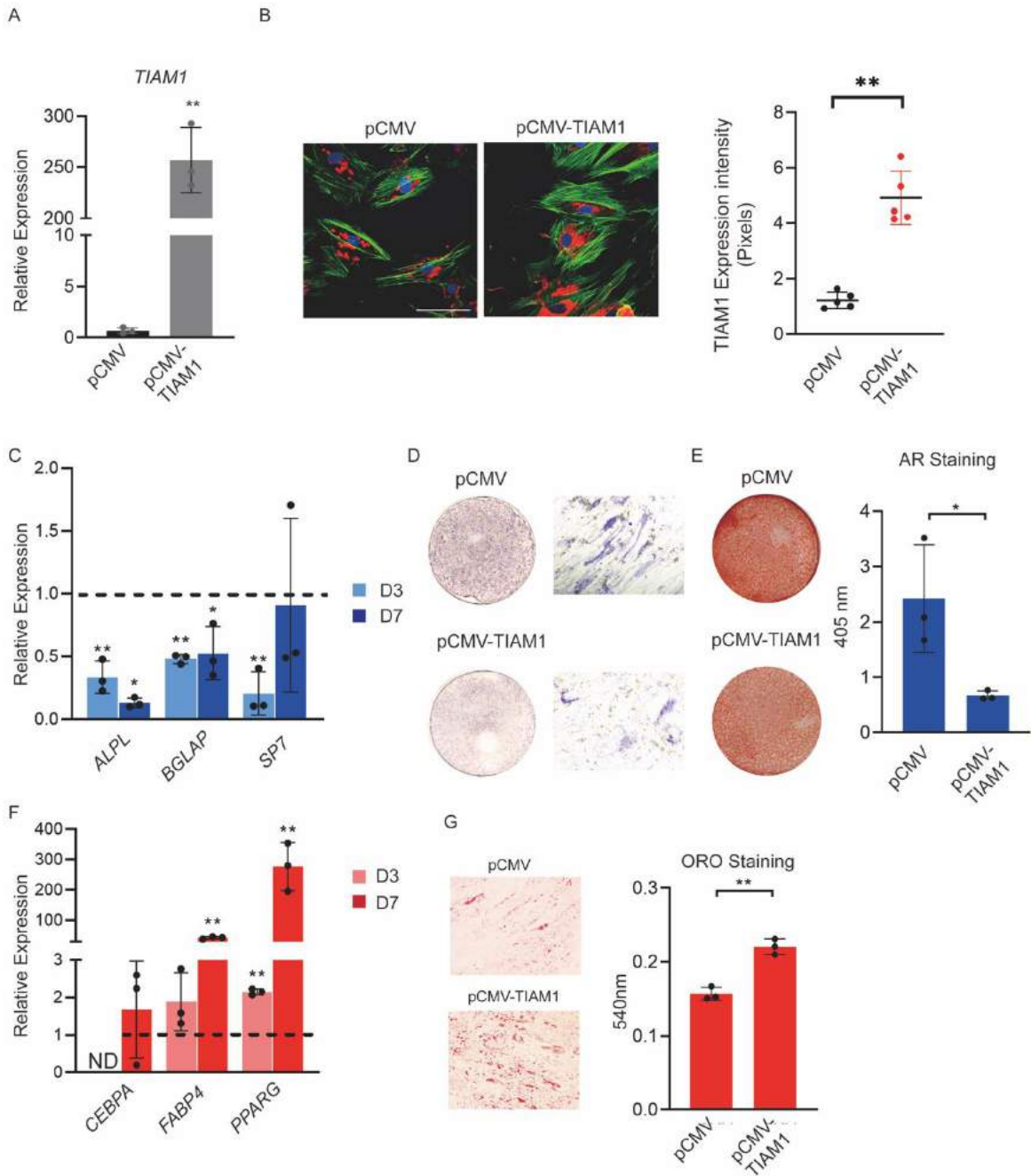
Figure 3. *TIAM1* **overexpression favors adipogenic over osteogenic differentiation of human adipose tissue-derived CD146⁺ pericytes. (A)** Validation of *TIAM1* overexpression (OE) by qRT-PCR, performed 48 hrs after treatment with *TIAM1* ORF plasmid (pCMV-TIAM1) or vector control (pCMV). **(B)** Validation of *TIAM1* overexpression by fluorescent immunocytochemistry for TIAM1 and semi-quantitative analysis, after 48 hrs. TIAM1 immunostaining appears red, while F-actin staining appears green. Random images (N=5) of fluorescent staining were obtained for semiquantitation of TIAM1 (Red) or F-actin (Green) area (mean Red or Green fluorescent area per field view). **(C)** Osteogenic gene markers at d 3 and 7 of osteogenic differentiation among *TIAM1* OE pericytes, assessed by qRT-PCR. Dashed lines indicate expression among pCMV vector control at the same timepoint. *ALPL:* Alkaline Phosphatase*; BGLAP: Osteocalcin; SP7: Osterix.* **(D)** Alkaline phosphatase (ALP) staining shown by whole well and representative 10x microscopical images on d 7 of differentiation. **(E)** Alizarin Red staining with quantification on d 10 of osteogenic differentiation, shown by whole well images. **(F)** Adipogenic gene marker expression at d 3 and 7 of adipogenic differentiation among *TIAM1* OE pericytes, assessed by qRT-PCR. Dashed lines indicate expression among vector control at the same timepoint. *CEBPA: CCAAT Enhancer Binding Protein Alpha; FABP4: fatty acid-binding protein 4; PPARG: peroxisome proliferator-activated receptor.* **(G)** Oil red O staining and quantification on d 10 of adipogenic differentiation (representative 10x magnification images shown). *$P<0.05$; **$P<0.01$ in comparison to pCMV vector control at the corresponding timepoint. Experiments performed in at least triplicate experimental replicates. Statistical analysis was performed using a two-samples Student's t-test. White scale bars: 20 µm.

769   **Figure 4.**

770
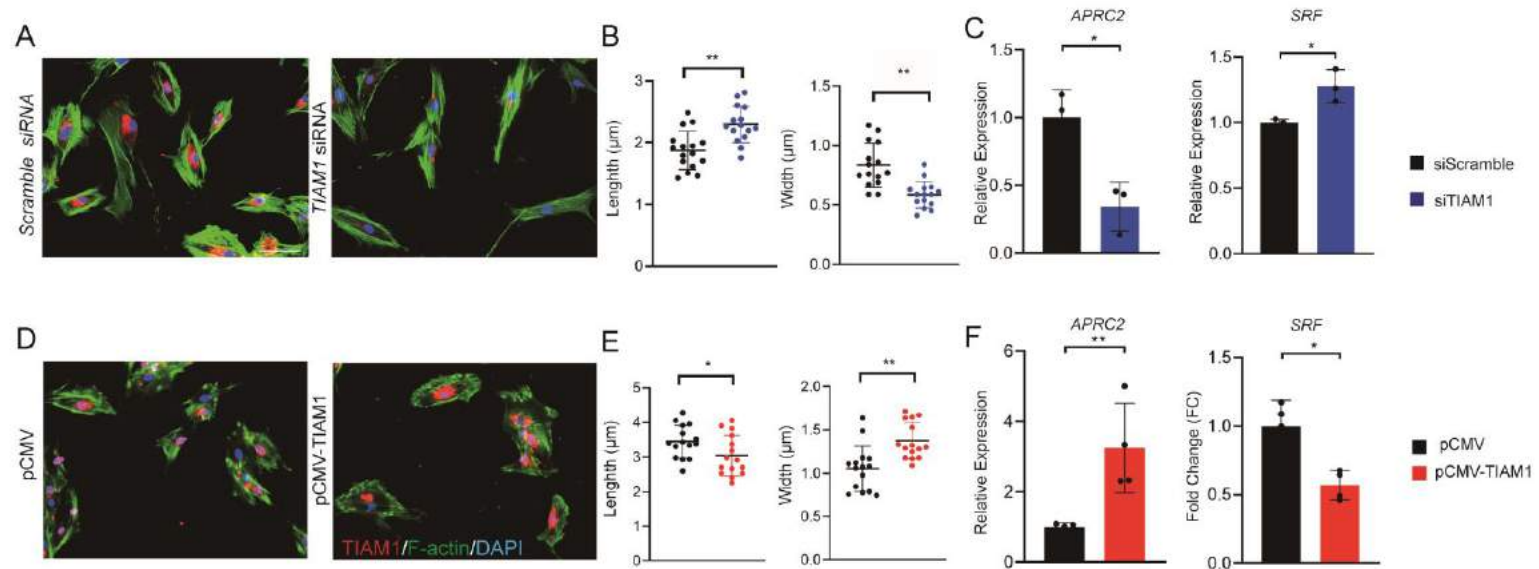
771

772

773

774

775

776

Figure 4: *TIAM1* **misexpression alters pericyte cellular morphology and gene targets of Rac1 and RhoA/ROCK signaling. (A)** Cellular morphology of human pericytes 48 hrs after treatment with *TIAM1* siRNA or Scramble siRNA. F-actin staining appears green, while TIAM1 immunostaining appears red. **(B)** Quantification of F-actin cell length and cell width among *TIAM1* siRNA or Scramble siRNA treated human pericytes. Each dot represents an individual cell, with images obtained from three random high magnification fields from each group. **(C)** Specific target gene expression for Rac1 (*ARPC2*) and RhoA/ROCK (*SRF*) signaling pathways among *TIAM1* siRNA or Scramble siRNA treated human pericytes, 24 hrs after treatment by qRT-PCR. *ARPC2*: Actin Related Protein 2/3 Complex Subunit 2; *SRF*: Serum response factor. **(D)** Cellular morphology of human pericytes 48hrs after incubation with *TIAM1* or control plasmids. F-actin staining appears green, while TIAM1 immunostaining appears red. **(E)** Quantification of F-actin angulation, cell length, and cell width among *TIAM1* or control plasmid treated human pericytes. Each dot represents an individual cell, with images obtained from three random high magnification fields from each group. **(F)** Specific target gene expression for Rac1 (*ARPC2*) and RhoA/ROCK (*SRF*) pathways, by qRT-PCR, 48hrs after treatment. *$P<0.05$; **$P<0.01$. Statistical analysis was performed using a two-way Student's t-test. White scale bars: 20 μm.

795

796   **Figure 5.**

797
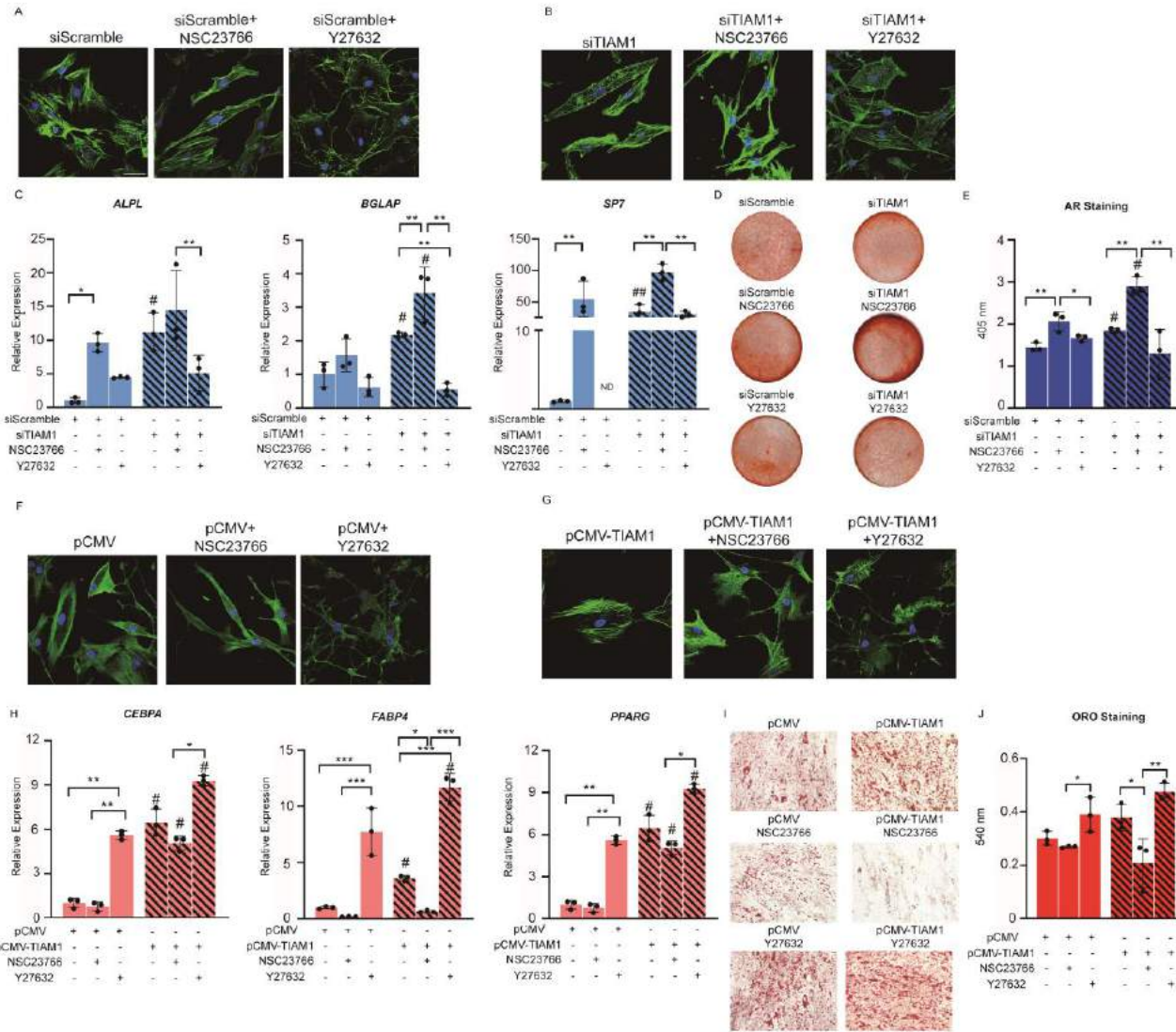
798 **Figure 5. Rac1 and ROCK inhibitors alter pericyte morphology and**

799 **osteo/adipogenic differentiation potential with *TIAM1* misexpression. (A,B)**

800 Pericyte morphology after 48 hrs treatment with NSC23766 (Rac1 inhibitor, 5 µM) or

801 Y27632 (ROCK inhibitor, 10 µM). F-actin appears green and DAPI staining appears blue.

802 Images shown of human pericytes with *TIAM1* KD or scramble siRNA. **(C)** Osteogenic

803 gene markers at d 7 of osteogenic differentiation among *TIAM1* KD or siRNA control

804 treated pericytes with NSC23766 or Y27632, as assessed by qRT-PCR. *ALPL: Alkaline*

805 *Phosphatase; BGLAP: Osteocalcin; SP7: Osterix*. **(D,E)** Alizarin Red staining and

806 quantification on d 10 of osteogenic differentiation. **(F,G)** Pericyte morphology with

807 treatment of NSC23766 (5 µM) or Y27632 (10 µM). F-actin appears green and DAPI

808 staining appears blue. Images shown of human pericytes with *TIAM1* OE or vector

809 control. **(H)** Adipogenic gene marker expression at d 7 of adipogenic differentiation among

810 *TIAM1* OE or vector control treated pericytes with NSC23766 or Y27632, as assessed by

811 qRT-PCR. *CEBPA: CCAAT Enhancer Binding Protein Alpha; FABP4: fatty acid-binding*

812 *protein 4; PPARG: peroxisome proliferator-activated receptor*. **(I,J)** Oil red O staining and

813 quantification on d 10. Representative images shown at 10x magnification. *, ** $P<0.05$;

814 $P<0.01$ between the groups. # $P <0.05$ in comparison to the corresponding treatment

815 group with siCramble/pCMV control. Each dot in the scatterplots represents an individual

816 well. Statistical analysis was performed using a two-way ANOVA followed by Tukey's post

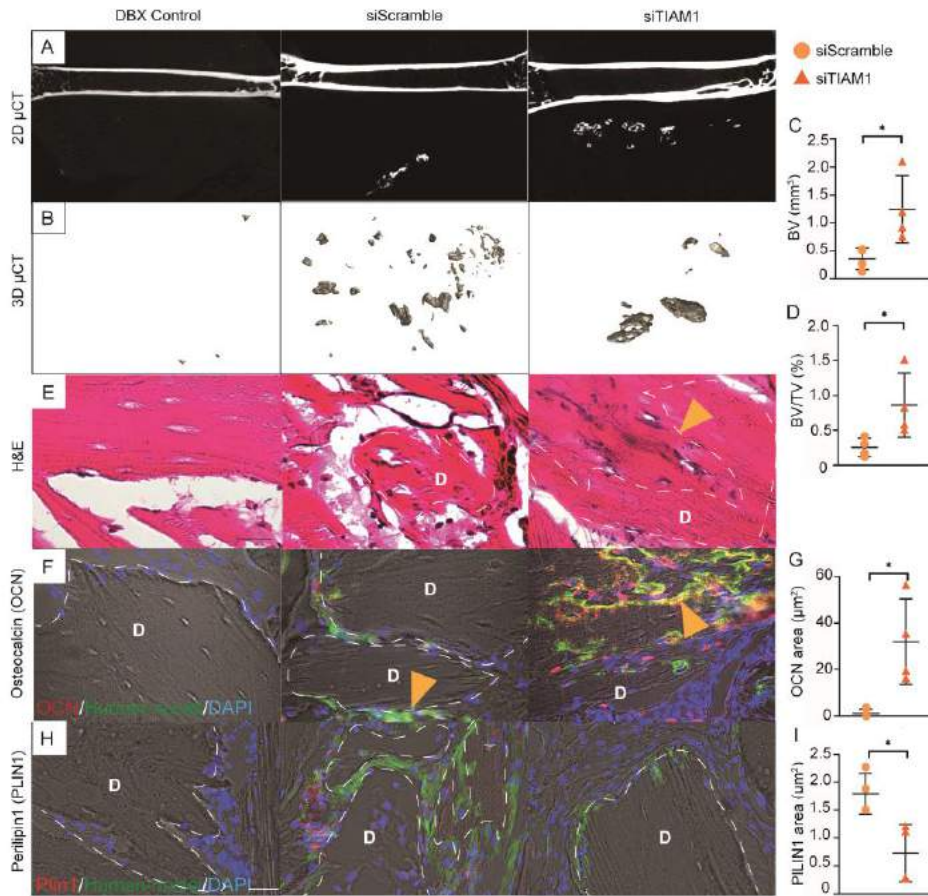817 hoc test. White scale bars: 20 µm.

818

819

820

821   **Figure 6.**

822
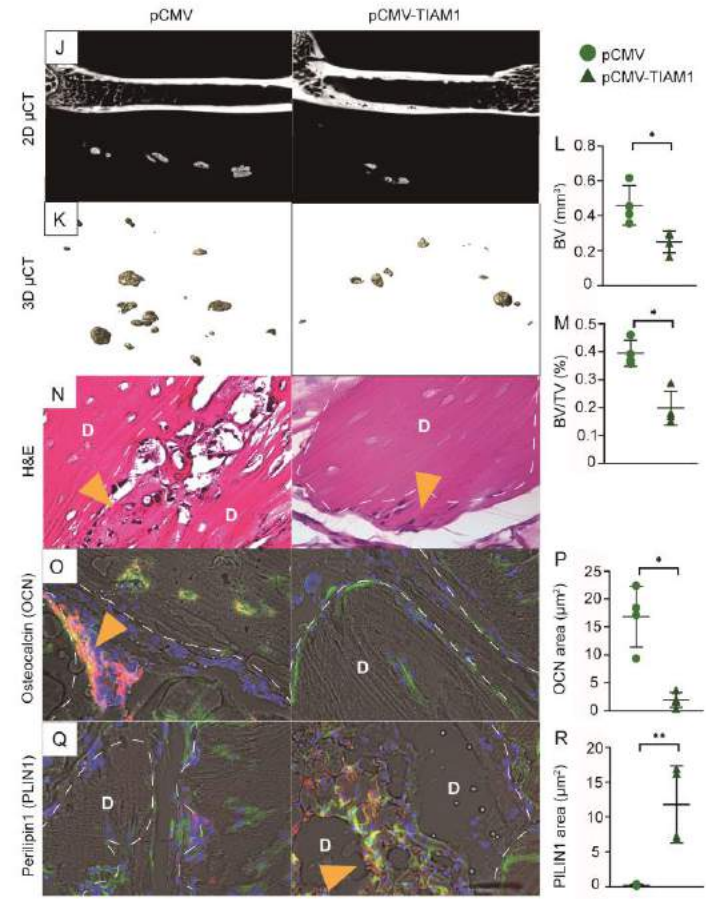
823

824 **Figure 6. *TIAM1* misexpression alters bone and adipose tissue generation after**

825 **human pericyte xenotransplantation.** *TIAM1* KD or OE pericytes or indicated control

826 were implanted subcutaneously in the dorsum of adult athymic nude male mice (Charles

827 River Laboratories (Strain Code:490) using a demineralized bone matrix carrier (3 million

828 cells / 50 mg DBX). Assessments were performed after 8 wks. **(A-K)** *TIAM1* KD pericyte

829 implants in relation to scramble siRNA pericytes. **(A)** Representative two-dimensional

830 µCT images, **(B)** three-dimensional µCT reconstructions, and quantification of **(C)** bone

831 volume (BV) and **(D)** fractional bone volume (BV/TV). Histology by **(E)** H&E staining. **(F)**

832 Osteocalcin (OCN) immunohistochemistry in red and Human Nuclei (HuNu) in green, with

833 **(G)** OCN quantification. **(H)** Perilipin 1 (Plin1) immunohistochemistry in red and Human

834 Nuclei in green (Yellow arrow point out cell co-express of both OCN and HuNu) and **(I)**

835 Plin1 quantification. **(J-R)** *TIAM1* OE pericyte implants in relation to pCMV vector control

836 pericytes. **(J)** Representative two-dimensional µCT images, **(K)** three-dimensional µCT

837 reconstructions, and quantification of **(L)** BV and **(M)** BV/TV. Histology by **(N)** H&E

838 staining. **(O)** OCN immunohistochemistry in red and HuNu in green, with **(P)** OCN

839 quantification. **(Q)** Plin1 immunohistochemistry in red and Human Nuclei in green, and

840 **(R)** Plin1 quantification. Dotted white lines demarcate edges of the DBX area = "D". Scale

841 bar: 20µm. All quantitative data normalized to acellular control (DBX control). Each dot

842 in the scatterplots represents an individual implantation site. N=4 implants per group.

843 *P<0.05; **P<0.01. Statistical analysis was performed using two-sample Student's t-

844 test.

845

Metadata of the article that will be visualized in OnlineFirst

1	Article Title	**Challenges and Perspectives on the Use of Pericytes in Tissue Engineering**
2	Article Sub- Title	
3	Article Copyright - Year	**Springer Nature Switzerland AG 2022** **(This will be the copyright line in the final PDF)**
4	Journal Name	Current Tissue Microenvironment Reports
5		Family Name	**Bertassoni**
6		Particle	
7		Given Name	**Luiz**
8		Suffix	
9		Organization	Oregon Health & Science University
10		Division	Biomaterials and Biomechanics, School of Dentistry
11		Address	2730 S.W. Moody Ave, Portland 97201, OR, USA
12		Organization	Oregon Health & Science University
13	Corresponding Author	Division	Department of Restorative Dentistry, School of Dentistry
14		Address	Portland, OR, USA
15		Organization	Oregon Health & Science University
16		Division	Department of Biomedical Engineering, School of Medicine
17		Address	Portland, OR, USA
18		Organization	Knight Cancer Institute
19		Division	Cancer Early Detection Advanced Research Center (CEDAR)
20		Address	Portland, OR, USA
21		e-mail	bertasso@ohsu.edu
22		Family Name	**Franca**
23		Particle	
24		Given Name	**Cristiane Miranda**
25		Suffix	
26		Organization	Oregon Health & Science University
27	Corresponding Author	Division	Biomaterials and Biomechanics, School of Dentistry
28		Address	2730 S.W. Moody Ave, Portland 97201, OR, USA
29		Organization	Oregon Health & Science University
30		Division	Department of Restorative Dentistry, School of Dentistry
31		Address	Portland, OR, USA
32		e-mail	mirandaf@ohsu.edu
33	Author	Family Name	**Hsu**

34	Particle	
35	Given Name	**Ginny Ching-Yun**
36	Suffix	
37	Organization	Oregon Health & Science University
38	Division	Department of Orthodontics, School of Dentistry
39	Address	Portland, OR, USA
40	Organization	Johns Hopkins University
41	Division	Department of Pathology, School of Medicine
42	Address	Baltimore, MD, USA
43	e-mail	
44	Family Name	**Lu**
45	Particle	
46	Given Name	**Amy**
47	Suffix	
48	Organization	Johns Hopkins University
49 Author	Division	Department of Pathology, School of Medicine
50	Address	Baltimore, MD, USA
51	Organization	Harvard Medical School
52	Division	Department of Orthopedic Surgery, Massachusetts General Hospital
53	Address	Boston, MA, USA
54	e-mail	

58	Abstract	**Purpose of Review:** The field of tissue engineering is driven by the need to provide functional equivalents of native tissues that can be used for implantation. Pericytes have great potential to be used in this regard because of their plasticity, as well as their role in angiogenesis, growth factor secretion, immunomodulation, and tissue repair. However, several questions about translational strategies using pericyte-supported vasculature or harnessing pericytes' plasticity to accelerate in vivo integration of engineered tissues remain.

Recent Findings: We first offer an overview of recent findings on pericytes' involvement in the formation, remodeling, and function of blood vessels, along with an analysis of the most common pericyte markers used in tissue engineering. Next, we discuss two distinct tissue engineering approaches related to the use of pericytes in which (i) pericytes' plasticity can be used as a source of mesenchymal cells or (ii) stem cells can be differentiated in contact with endothelial cells (ECs) to engineer pericyte-supported vasculature. Finally, we provide a perspective on current challenges and future directions for the use of pericytes in tissue fabrication.

Summary: We anticipate that combining a thorough, mechanistic understanding of the natural formation of pericyte-supported vasculature in the body with an overview of existing methods and challenges related to the fabrication of engineered blood vessels may provide the fundamental

		knowledge necessary to develop better approaches to engineering functional, long-lasting vasculature and tissues.
59	Keywords separated by ' - '	Stem cells - Differentiation - Pericyte - Tissue engineering - Vascular biology
60	Foot note information	This article is part of the Topical Collection on *Pericytes*
		Springer Nature remains neutral with regard to jurisdictional claims in published maps and institutional affiliations.

PERICYTES (A BIRBRAIR, SECTION EDITOR)

Challenges and Perspectives on the Use of Pericytes in Tissue Engineering

Ginny Ching-Yun Hsu[1,2] · Amy Lu[2,3] · Luiz Bertassoni[4,5,6,7] · Cristiane Miranda Franca[4,7]

Abstract

Purpose of Review The field of tissue engineering is driven by the need to provide functional equivalents of native tissues that can be used for implantation. Pericytes have great potential to be used in this regard because of their plasticity, as well as their role in angiogenesis, growth factor secretion, immunomodulation, and tissue repair. However, several questions about translational strategies using pericyte-supported vasculature or harnessing pericytes' plasticity to accelerate in vivo integration of engineered tissues remain.

Recent Findings We first offer an overview of recent findings on pericytes' involvement in the formation, remodeling, and function of blood vessels, along with an analysis of the most common pericyte markers used in tissue engineering. Next, we discuss two distinct tissue engineering approaches related to the use of pericytes in which (i) pericytes' plasticity can be used as a source of mesenchymal cells or (ii) stem cells can be differentiated in contact with endothelial cells (ECs) to engineer pericyte-supported vasculature. Finally, we provide a perspective on current challenges and future directions for the use of pericytes in tissue fabrication.

Summary We anticipate that combining a thorough, mechanistic understanding of the natural formation of pericyte-supported vasculature in the body with an overview of existing methods and challenges related to the fabrication of engineered blood vessels may provide the fundamental knowledge necessary to develop better approaches to engineering functional, long-lasting vasculature and tissues.

Keywords Stem cells · Differentiation · Pericyte · Tissue engineering · Vascular biology

Introduction

The term "perivascular cell" mainly encompasses two cell types with somewhat overlapping characteristics: vascular smooth muscle cells and pericytes. Vascular smooth muscle cells surround and circumferentially wrap around large vessels, such as the aorta, carotid artery, and saphenous vein, while pericytes surround the microvasculature, such as capillaries, post-capillary venules, and terminal arterioles [1•, 2, 3].

Pericytes are cells present in nearly all vertebrate tissues in the abluminal side of microvascular endothelial cells (ECs), such as pre-capillary arterioles, capillaries, and postcapillary

✉ Luiz Bertassoni
  bertasso@ohsu.edu

✉ Cristiane Miranda Franca
  mirandaf@ohsu.edu

1 Department of Orthodontics, School of Dentistry, Oregon Health & Science University, Portland, OR, USA

2 Department of Pathology, School of Medicine, Johns Hopkins University, Baltimore, MD, USA

3 Department of Orthopedic Surgery, Massachusetts General Hospital, Harvard Medical School, Boston, MA, USA

4 Division of Biomaterials and Biomechanics, Department of Restorative Dentistry, Oregon Health & Science University, Portland, OR, USA

5 Department of Biomedical Engineering, School of Medicine, Oregon Health & Science University, Portland, OR, USA

6 Cancer Early Detection Advanced Research Center (CEDAR), Knight Cancer Institute, Portland, OR, USA

7 ~~Biomaterials and Biomechanics, School of Dentistry, Oregon Health & Science University, 2730 S.W. Moody Ave, Portland, OR 97201, USA~~

venules [4]. In certain tissues, pericytes acquire specialized functions and names, i.e., mesangial cells in kidney glomeruli and Ito cells in the liver. In general, pericytes are located around EC junctions embedded within the microvascular basement membrane, forming "umbrella-like" structures that cover the gaps between ECs [5]. Though pericyte morphology can differ greatly by location, these cells typically present an elongated, stellate-shaped cytoplasm, major processes oriented parallel to the long, vascular axis, and smaller protrusions that are circumferential and partially encircle the vessel wall [6]. A single pericyte can establish contact with several ECs and may extend its processes to more than one capillary, integrating signals as well as establishing a structural mechanism for contractile force transmission along the length of one or multiple vessels [7].

Pericytes have several functions in maintaining tissue homeostasis such as (a) vessel stabilization [3, 8]; (b) regulation of vascular tone, contractile capacity, transport, and permeability [9, 10]; (c) control of mechanisms that drive vessel quiescence, proliferation, sprouting, and regression [2, 11–13]; (d) synthesis of extracellular matrix proteins [14]; (e) immunologic functions [15]; (f) coagulation [16]; and (g) plastic potential to differentiate into some mesenchymal cell lineages [17, 18]. For detailed reviews, see [1•, 6].

In this review, we first offer an overview of pericytes' involvement in the formation, remodeling, and function of blood vessels along with an analysis of the most common pericyte markers used for tissue engineering purposes. Next, we discuss two distinct tissue engineering approaches related to the use of pericytes in which (i) their plastic potential can be used as a source of other cells for tissue regeneration or (ii) mesenchymal stem cells (MSCs) can be differentiated in contact with ECs to engineer pericyte-supported vasculature. Finally, we provide a perspective on current challenges and future directions for pericyte use to fabricate tissues. We anticipate that a thorough understanding of the mechanisms of the natural formation of pericyte-supported vasculature in the body, combined with an overview of existing methods and challenges related to the fabrication of engineered blood vessels, may provide the fundamental knowledge necessary to develop better approaches to engineering functional long-lasting vasculature.

Pericytes and Vasculature Formation

The process of creating vascular networks involves basically two sequential steps: vasculogenesis, the de novo formation of blood vessels from progenitor cells, and angiogenesis, which is the migration, branching, and pruning of an existing blood vessel to form additional vascular networks and capillary beds [19, 20]. During embryogenesis, the primitive ECs, derived from the mesodermal layer, migrate to form cell aggregates known as blood islands. Blood islands are capable of differentiating toward either hematopoietic or angioblastic lineages. As these cells begin to differentiate, they align with angioblasts on the outsides of blood islands and hematopoietic cells in the central core [20]. Angioblasts in the outer lining flatten and form intercellular connections to create a circumferential layer of primitive ECs, corresponding to the first stage of vessel formation. As the blood vessel matures, the endothelial layer forms a confluent, monocellular layer in contact with blood, and pericytes are recruited to coat the vessel. This promotes an anti-angiogenic effect, which stabilizes the vessel and limits further proliferation or migration of ECs [7]. This EC-pericyte signaling is mediated by direct cell-cell contact, the release of growth factors, and the modulation of the extracellular matrix [21]. Furthermore, the physical contact between ECs and pericytes is thought to induce a quiescent, non-sprouting phenotype [19, 20].

For pre-exiting vessels, angiogenesis occurs via sprouting or intussusception to generate new microvessels. Angiogenic sprouting is controlled by the balance between pro-angiogenic and quiescence signals, such as vascular endothelial growth factor (VEGF) and tight pericyte contact, respectively [21]. In conditions that favor angiogenesis, some ECs within the capillary vessel wall are selected for sprouting. These ECs, known as the tip cells, flip their apical-basal polarity, acquiring a motile and invasive activity which leads the growing sprout. Tip cells release platelet-derived growth factor B (PDGFB) to recruit pericytes to the new sprouts, since EC-EC junctions need to be maintained after lumen formation to prevent excessive leakage [22]. Activated pericytes in the parent vessel increase their volumes while shortening their processes, proliferate, detach from the vessel wall, and invade the newly vascularized tissue toward the growing front of the endothelial sprouts. In addition, pericytes can also be recruited by the differentiation of surrounding mesenchymal precursors or by their migration from the mural wall of the adjacent vessel. Subsequently, the migrating ECs reassemble to produce lumen and eventually mature in a stepwise transition from an actively growing vascular bed to a quiescent, fully formed, and functional network. A prominent and widely recognized feature of this maturation program is the recruitment of mural cells, either pericytes or vascular smooth muscle cells, to stabilize the vessels and prevent regression of the newly-formed vasculature [7, 19].

Pericyte Markers Often Used in Tissue Engineering

Pericytes are commonly identified based on their morphologies and locations through light and electron microscopy [1•]. Currently, there is no single gene or protein known to unequivocally identify these cells because the expression of

each marker may change according to the species, vessel type, segment of the microvasculature, tissue, and stage of the vessel (quiescent or angiogenic) [6]. Pericytes share some surface markers with MSCs and possess plasticity to differentiate into further mesenchymal cell types [23, 24••, 25, 26]. The most commonly used markers to identify pericytes are contractile proteins such as CD146, alpha smooth muscle actin (αSMA), nestin and desmin, or cell surface proteins such as neuron-glial 2 (NG2), platelet-derived growth factor receptor beta (PDGFRβ) [27], CD146 [28], aminopeptidase N (CD13) [29], or even some MSC markers, such as CD44, CD90, and CD105 [30]. However, these proteins can also be detected in additional cell types depending on their developmental stage [31], so pericytes are usually defined by using a combination of well-preserved tissue morphology, counter-labeled ECs, and one or two gene or protein markers (Fig. 1) [1•].

For pericytes derived from adipose tissue in particular, such heterogeneity in cell markers suggests a continuum of phenotypes (as subsets of cells at various stages of differentiation), due to their fate dynamics [31]. Single-cell analysis has been used to identify and reveal the specific markers or signaling pathways that might contribute to diverse, multiple functions among adipose-derived pericytes. Recently, a study investigated the occurrence of related groups of genes, or "metagenes," in pericytes and adventitial perivascular cells to determine their transcriptional identities. Such an approach was used as a complement to the common practice of seeking gene "markers" to establish a cell's identity and its changes during differentiation, which may or may not be inscribed in individually transcribed genes. To that end, human adventitial perivascular cells and pericyte were used for single-cell analysis and demonstrated that the expression of 7 genes for pericytes (*ACTA2*, *FABP4*, *ITGA1*, *MCAM*, *RGS5*, *SORT1*, and *TPM1*) and 15 genes for adventitial perivascular cells (*CD34*, *CDH11*, *CHL1*, *CXCL12*, *EGFR*, *FGF7*, *FGF10*, *IGFBP3*, *GHR*, *MME*, *MMP2*, *NOX4*, *PDGFD*, *PDGFRA*,

Fig. 1 Schematic highlighting some of pericytes' biological functions and surface markers. Pericytes are present in nearly all tissues being located on the in the abluminal side of microvascular endothelial cells. Pericytes express different cell markers and possess several biological functions such as vessel stabilization, control of vessel permeability, and sprouting. Furthermore, pericytes present a plastic potential which plays an important role in tissue repair and development (original image)
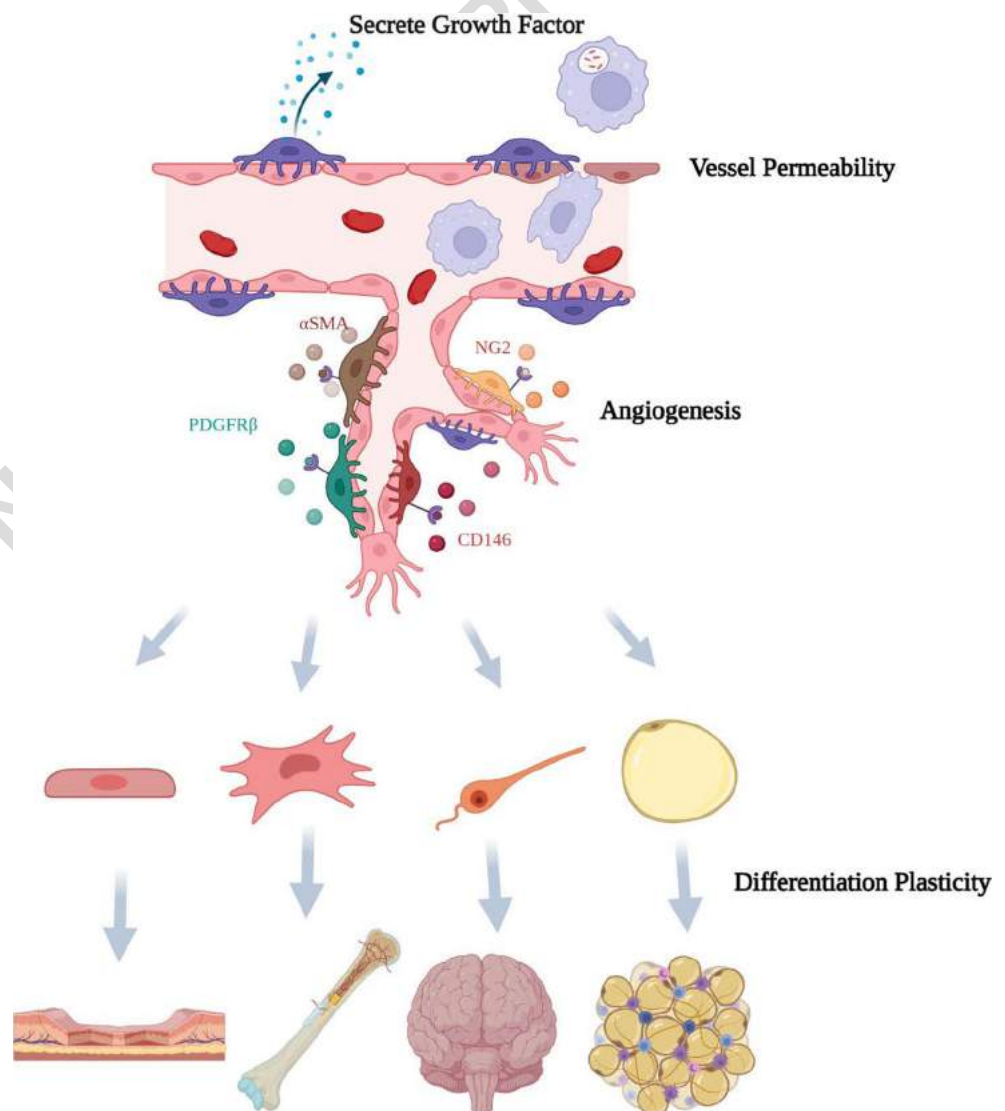
and *SFRP2*) were distinct between the two cell types. Overall, these genes can be classified in hierarchies tightly related to five categories with broadly distributed functions, (a) maintenance of, or release from stemness; (b) transcriptional control; (c) plasma membrane and glycocalyx properties; (d) cytoskeletal reorganization; and (e) extracellular matrix degradation. These results indicate that adventitial perivascular cells and pericytes can be separated on the basis of surface marker expression and single-cell transcriptional profiling. Moreover, the complex compartmentalization of their gene expressions suggests that both cells are primitive, presenting plastic potential, having their subpopulations show diverse contributions to tissue renewal and repair [31].

CD146, also known as cell surface glycoprotein MUC18 or MCAM (melanoma cell adhesion molecule), is a transmembrane glycoprotein and a member of the immunoglobulin superfamily [32]. CD146 regulates the activation of PDGFRβ and is associated with endothelial integrity, particularly due to its role in pericyte recruitment during angiogenesis [33, 34]. CD146+CD34−CD31−CD45− pericytes are characterized as osteogenic progenitor cells and are the most commonly purified pericytes used for orthopedic research [24••, 26, 35–38]. For instance, adipose-derived CD146+CD34−CD31−CD45− pericytes have shown stronger osteogenic properties compared to their CD146−CD34−CD31−CD45− counterparts in vivo [24••]. The bone healing and ectopic bone formation capabilities of CD146+ pericytes have also been validated in murine calvarial defect [36, 39] and intramuscular implantation models [40].

PDGFRβ is a co-receptor for CD146 and is predominately expressed on microvasculature, functioning in vessel stabilization and pericyte recruitment. Mice deficient in PDGFβ or its ligand PDGF-B have markedly reduced pericyte numbers, and subsequent aneurisms, edema, and embryonic death [34]. Our group used PDGFα+ and PDGFβ+ pericytes in a murine model of osteoarthritis with destabilization of the medial meniscus (DMM) to investigate the differential effects of these two cell populations in the alleviation of osteoarthritis [41]. Cells were isolated from transgenic PDGFα+ and PDGFβ+ CreER^{T2} reporter animals and delivered as single, intra-articular doses to mice after the meniscus injury. PDGFRβ+ CD146+ pericytes were able to deposit and differentiate into diverse tissues within the knee, preventing subchondral sclerosis, while PDGFα+ had no effect on the meniscal lesion [41] (Fig. 2).

PDGFRα, or CD140, is a cell surface tyrosine kinase receptor that is expressed by perivascular cells in the bone marrow, heart, skeletal muscle, adipose tissue, and brain [42–44]. Similar to PDGFRβ, PDGFRα plays an important role in cell differentiation and tissue repair. Pericytes that expressed PDGFRα demonstrated more plasticity than those that did not express the receptor [44]. Upon implantation with bone graft material, PDGFRα$^+$ cells presented more

osteoblastogenic properties than PDGFRα$^−$ perivascular cells [45]. However, the plastic properties of PDGFRα$^+$ cells have only been validated in adipose- and bone-derived perivascular cells [41].

NG2, a proteoglycan first described in the neural system, is a marker of mature pericytes. NG2 has been shown to have an important role in angiogenesis, where it promotes EC migration and proliferation [15, 46]. NG2 is expressed on newly formed vessels in normal conditions and also during tissue repair and tumor angiogenesis [47, 48]. Indeed, NG2 expression distinguishes three subsets of human pericytes: those associated with capillaries (NG2+ αSMA−), venules (NG2− αSMA+), and arterioles (NG2+ αSMA+) [18, 49]. NG2 is one of the most commonly used markers for pericytes in studies that engineer pericyte-supported vasculature [50–52].

Alpha smooth muscle actin (αSMA) is a marker for active pericytes, smooth muscle cells, and myofibroblasts, and its presence is correlated with blood vessel contractility, blood pressure control, and tissue repair or inflammation [1•, 53]. Quiescent pericytes from the central nervous system usually do not express αSMA [1•], although αSMA can be present in tissue repair after brain ischemic strokes [53]. Along with NG2, αSMA is another frequently used marker for pericyte-supported engineered vessels [54–59].

There is a subpopulation of perivascular cells present from microvascular capillaries to large vessels in several organs that expresses Gli1, a transcriptional factor for hedgehog signaling. Despite not being a typical marker for pericytes, Gli1$^+$ cells present typical MSC markers and possess trilineage differentiation capabilities toward chondrogenic, adipogenic, and osteogenic lineages [60]. Interestingly, all Gli1$^+$ cells express PDGFRβ+, but they represent only a small fraction of the total PDGFRβ+ perivascular population [60]. Recently, these Gli1$^+$ cells have gained attention because in vivo fate tracing experiments in the heart, lung, kidney, and liver revealed that after organ injury, Gli1$^+$ proliferated in the perivascular space and differentiated into αSMA+ myofibroblasts. Conversely, these cells do not express NG2 in homeostasis of fibrosis, but acquire NG2 expression during angiogenesis. Moreover, removing the first intron of Gli1 in human embryonic stem cells (hESCs) reduces their osteogenic property and hematopoietic potential [61]. Evidence also shows that Gli1$^+$ cells play an important role in vessel calcification [62], organ fibrosis [60], and other tissue repair involved in pathological conditions [63]. Gli1$^+$ cells are essential for tissue development and homeostasis, and Gli1 is a promising marker to isolate very specific pericytes for tissue engineering. However, only a few studies have used these cells for in vitro bone engineering [64].

Such variability in marker expression and cell morphology has led to the evidence that pericytes represent a heterogeneous cell population [14, 65–67]. Birbrair et al. identified two pericyte subtypes based on the expression of Nestin and NG2 [14]. Those
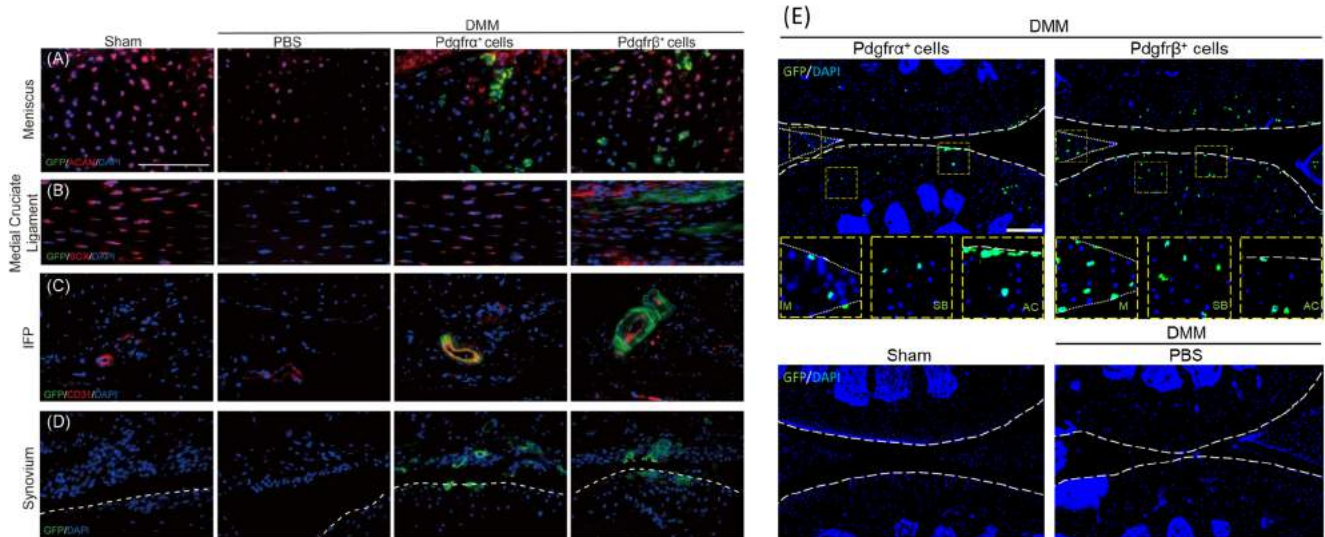
Current Tissue Microenvironment Reports

Fig. 2 Cell engraftment of GFP-PDGFRα⁺ and PDGFRβ⁺ pericytes in destabilization of the medial meniscus (DMM) surgical mice showed differential tissue deposition in the intra-articular space after 8 weeks. Immunofluorescent staining of **A** aggrecan (ACAN) in the meniscus, **B** scleraxis (SCX) in the medial cruciate ligament (MCL), **C** CD31 in the infrapatellar fat pad (IFP), **D** joint capsule, and **E** articular cartilage: meniscus (M), subchondral bone (SB), and superficial articular cartilage (AC). Reproduced with permission from Hsu et al. [41]

subtypes, named types 1 and 2, are present surrounding blood vessels in the lungs, kidneys, heart, spinal cord, and brain and respond differently to tissue injury. For instance, type-1 pericytes accumulate after tissue injury and produce collagen, being considered a potential target for anti-fibrotic therapies, while type 2 pericytes participate in muscle regeneration [14, 68, 69]. Conversely, other authors refer to subpopulations of pericytes from the central nervous system as type A and B, in which type A expresses PDGFRβ and CD13, while type B can be distinguished by the expression of desmin and/or αSMA [67]. Type A pericytes have a role in generating fibrotic scars in lesions of the central nervous system and also contribute to brain tumor stroma [65]. Further studies revealed that subpopulations of CD146+ pericytes can promote neurogenic differentiation, and NG2+ pericytes participate in angiogenesis [70]. Still, there is much to understand regarding the heterogeneity of pericytes and how such heterogeneity could be honed to improve the outcomes in tissue engineering therapeutics. Collectively, a major concern that arises from those studies is that a subset of pericytes would be prone to induce fibrosis, and if this is not a desired outcome in tissue engineering strategies, this potential setback would have to be considered.

Use of Pericytes and Perivascular Cells in Tissue Engineering

Pericytes' Plasticity and Pericytes as Sources of Mesenchymal Cells

Pericytes possess plastic potential and are considered to be a source of other cells in multiple organs in response to injury or during homeostasis, as demonstrated by lineage tracing in vivo studies [71]. Although pericytes have been shown to be quiescent, slow-cycling cells in some tissues [72•], while in the angiogenic state, they become highly proliferative with the ability to self-renew and originate daughter cells with considerable mesenchymal potential in vitro and in vivo [6]. In the presence of inflammation, repair, or another event that disrupts vascular stability, pericytes can dissociate from ECs and migrate toward the interstitial tissue as cells resembling MSCs in morphology, growth, surface markers, and clonal multilineage differentiation [24••, 26, 40, 73]. Descendant cells of the dissociated and migrating pericytes are highly proliferative, with transit-amplifying phenotypes and demonstrated abilities to differentiate into cells with adipogenic [74], osteogenic [75, 76], chondrogenic [77], and myogenic phenotypes [18]. Moreover, pericytes display additional indirect properties, such as paracrine secretion of growth factors, immunomodulation, regulation of postinjury tissue remodeling, and activation of endogenous repair/regeneration mechanisms that play an important role for pericyte-based cell therapy with great potential for regenerative medicine [25, 40, 78, 79].

Pericytes were first used in tissue engineering efforts in the 1970s [1•]. Since then, despite different studies suggesting the multipotency of pericytes, they have been predominately used in vessel regeneration and orthopedic tissue engineering [35]. The osteogenic potential of pericytes was discovered due to growing evidence of their role in vessel constriction and calcification [80]. Since then, these cells have been used in orthopedic tissue engineering, especially in the context of bone repair. James et al. purified pericytes from human lipoaspirate, seeded them into scaffolds of either collagen or demineralized bone matrix, and implanted the purified cells in athymic mice.

They found that human pericytes undergo significantly robust bone formation in comparison to unsorted populations of stromal cells from the same patient [24••]. Chung et al. demonstrated that implanted human adipose tissue (AT)-derived pericytes could positively regulate native bone formation by increasing angiogenesis [79]. Likewise, pericyte implantation has also been shown to prevent atrophic nonunion in nonunion tibial rat models [81]. Critical-size calvaria defect models in nonobese diabetic/severe combined immunodeficiency (NOD/SCID) mice demonstrated a synergetic effect of CD146+ pericytes and CD34+ adventitial cells in bone formation and angiogenesis [36]. Ectopic bone formation mouse models have shown the osteogenic differentiation capabilities of human adipose tissue-derived CD146+ pericytes in vivo [35]. Moreover, the utility of pericytes for engineering other mesenchymal tissues, such as skeletal and cardiac muscle, has been well-documented in vitro and in preclinical animal models [25, 28, 40, 82].

However, the cell fate plasticity of endogenous pericytes has been challenged by a work by Guimaraes-Camboa et al., which investigated the expression of the transcriptional factor *Tbx18* in different organs in homeostasis and disease [72•]. *Tbx18* is a gene selectively expressed in the pericytes and vascular smooth muscle cells of specific organs in adult mice, including the retina, brain, heart, skeletal muscle, and white and brown fat depots. Therefore, the authors generated a *Tbx18*-CreETR2 murine line that allowed for the genetic labeling of pericytes and vascular smooth cells in intact tissues. Pericytes were tracked in the animals for 2 years during aging, obesity, cardiac fibrosis, and in the skeletal muscle. Two main findings stood out. First, the progeny of *Tbx-18*-CreETR2-derived pericytes maintained their mural identity in the heart, skeletal muscle, brain, and fat. Second, cells from *Tbx-18*-derived pericytes might contribute to fibrosis by adopting an activated state in response to injury, without significantly contributing as progenitors of other cell lineages [72•]. Collectively, the evidence in this study strongly suggests that, in vivo, pericytes do not behave as stem cells [23]. Yet, this study did not test if *Tbx-18*-CreETR2-derived pericytes could give rise to other cell lineages such as osteoblasts, chondrocytes, or odontoblasts.

Several questions related to pericyte plasticity in vivo still remain, since it has been suggested by other studies that pericytes from different organs or with different molecular signatures present different plastic potential [23]. Dellavalle et al. used Alkaline Phosphatase-CreERT2 transgenic mice to demonstrate that pericytes residing in postnatal skeletal muscle differentiate into skeletal muscle fibers and generate satellite cells, the skeletal muscle-specific progenitors [83]. Sacchetti et al. demonstrated that muscle pericytes are not spontaneously osteochondrogenic, but rather, present markers and behaviors coincident with an ectopic perivascular subset of committed myogenic cells similar to satellite cells [84]. In

conclusion, the plastic potential of pericytes is far from being completely understood, and future studies using new pericyte lineage tracing strategies may disclose a more predictable role for pericytes as progenitors of other cell lines in homeostasis and disease [23].

Pericytes to Engineer Vascularized Tissues

The field of tissue engineering is driven by the need to provide functional equivalents of native tissues that can be used for implantation. Arguably, successful strategies to fabricate vascularized tissues need to guarantee that engineered vessels are functional, stable, long-lasting, and able to promptly anastomose to the host vasculature to avoid the graft undergoing core necrosis [85, 86]. The survival and integration of tissue-engineered constructs depends on the rapid and efficient formation of an organized and perfusable microvascular network evenly distributed inside the scaffold [86]. However, engineered vessels from EC monocultures tend to be immature, leaky, unstable, and prone to regression in a few days [85]. To engineer vascular networks with extended lifespans and improved functions, a number of strategies have been studied, such as genetic manipulation [87], creating scaffolds with different compositions [88], and using various combinations of growth factors [89–91]. In 2004, a seminal work by Koike et al. [85] used a co-culture of human umbilical vein ECs (HUVECs) and mesenchymal precursor cells in a three-dimensional fibronectin/type I collagen gel to create long-lasting vasculature in vivo. After the implantation of the constructs in mice, the temporal changes of engineered and host vessels were investigated using intravital, multiphoton laser-scanning microscopy. This showed that engineered mesenchymal cells differentiated into mural cells through heterotypic interactions with ECs, creating chimeric vessels that lasted for 1 year [85]. This work paved the way for following investigations on the use of perivascular cells to promote the formation of microvascular networks within tissue engineering constructs. Since then, pericytes [92], fibroblasts [93, 94], and MSCs [95] have been cultured to accelerate self-assembly and stabilization of the engineered vasculature with promising results (Fig. 3).

The anastomosis of engineered HUVEC microvessels with the host cells happens via a process termed "wrapping-and-tapping," where implanted HUVECs first wrap around the pre-existing host vessels and replace segments of them to redirect blood flow into the implanted vasculature [51]. In this study, Cheng et al. identified the cellular interactions that result in anastomosis of implanted vascular networks with the host vasculature. The authors found that vessels formed by the transplanted ECs replaced segments of host vessels near the gel-tissue interface. Moreover, host vessels that had not been wrapped by transplanted HUVECs remained surrounded by a regularly distributed layer of NG2+ pericytes. Conversely, host
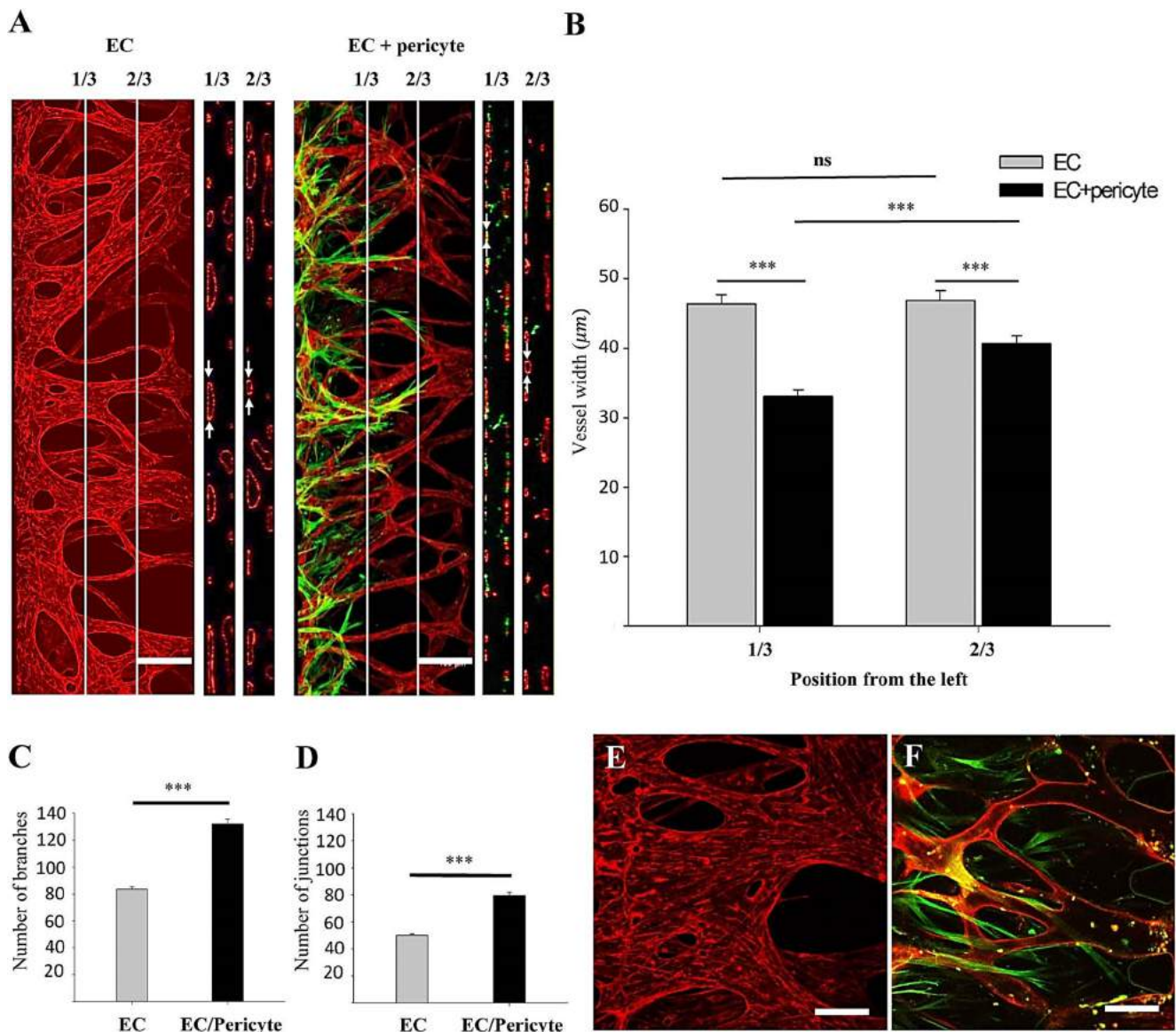
Fig. 3 Characterization of vascular morphological properties and comparison of EC monocultures and EC-pericyte co-cultures. **A** The 3D confocal image sectioned along the lines that divide the width of the ROI into three equal parts. Cross-sectional view of each portion clearly shows lumen formation of the blood vessel network (white arrows). **B** Vessel widths were measured along the sectioned lines. When two cells were cultured together, vessel width decreased significantly. The width of the pericyte-covered vessel increased again at the point region. **C, D** The numbers of junctions and branches increased significantly under co-culture conditions. The protective effect of pericytes from vessel dilation was significant when compared with the EC-only vessel at day 7 (**E**) and the pericyte-covered vessel at day 11 (**F**). CD31 (red) shows staining of ECs and α-SMA (green) shows staining of pericytes. Scale bar, 200 μm (**A, B**) or 100 μm (**E, F**) ($n = 28$ for EC monocultures, $n = 26$ for EC-pericyte co-cultures. *** $p < 0.001$). Reproduced with permission from Kim et al. [59]

447 vessels that anastomosed with engrafted vessels exhibited a
448 highly disorganized pattern of NG2$^+$ pericytes in the wrapping
449 segment, with a significant correlation between a disruption of
450 pericyte morphology and the presence of wrapping HUVECs.
451 At each step of the anastomosis, ECs integrated signals from
452 the environment, such as microanatomic information and solu-
453 ble agents, to determine behavior. Once perfused, transplanted
454 vessels matured, becoming increasingly covered by normal
455 NG2$^+$ pericytes. Collectively, these results indicate that a better
456 understanding of such microenvironmental cues and how they

457 are integrated by ECs and pericytes is fundamental for devel-
458 oping more effective and precise strategies for modulating vas-
459 culogenesis and angiogenesis [51].
460   Mechanical properties of the tissue are long-known to drive
461 stem cell fate [96]. A challenge for engineering microvascular
462 networks is that scaffolds with stiffness values above 3 kPa,
463 especially those composed of methacrylated gelatin
464 hydrogels, can be inhibitory for the self-assembly of vascula-
465 ture (Fig. 4A–D) or lead to the formation of leaky vessels (Fig.
466 4A–D) independent of pericyte presence [97].
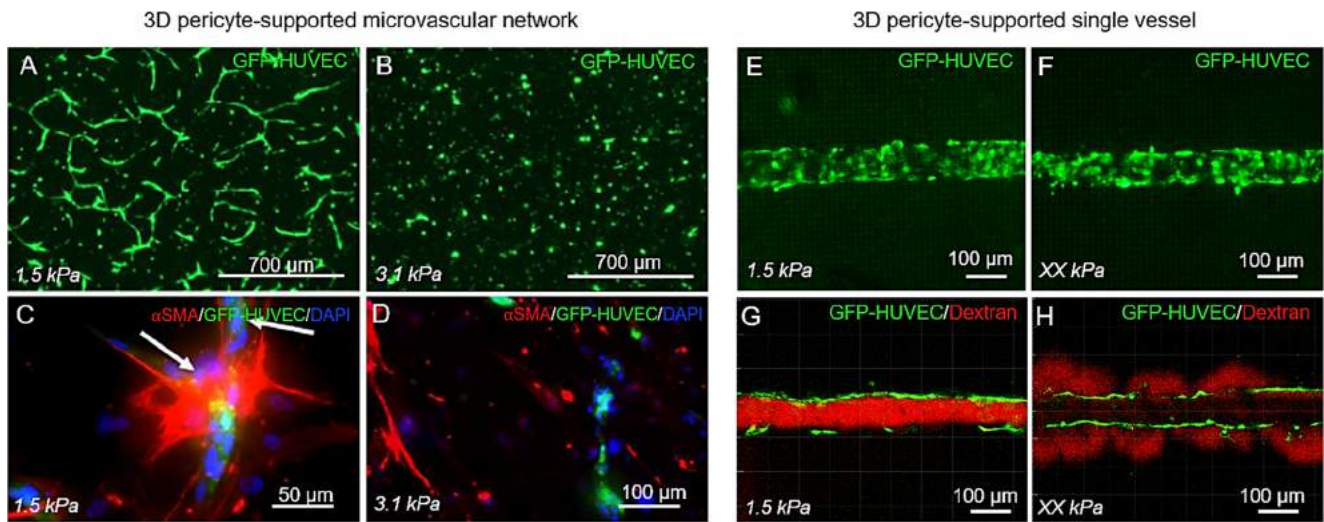
Fig. 4 Effect of stiffness on engineered pericyte-supported vasculature. **A** Softer hydrogels promote the assembly of microvascular networks within 3 days (5% GelMA, 0.05% lithium acylphosphinate—LAP, co-culture of stem cells from apical papilla—SCAPs and HUVECs, 1:4 ratio, 5×10^6 cells/mL), while **B** vasculature formation was not observed for stiffer hydrogels (5% GelMA, 0.1% LAP, similar cell conditions). Likewise, more pericyte differentiation was detected in the softer hydrogels (**C**) when compared to stiffer hydrogels (**D**). Reproduced with permission from Monteiro et al. [97]. Matching results are observed when pericyte-supported single vessels are fabricated in collagen gels with different fibrillogenic temperatures, which lead to variable stiffnesses. **E** Single vessels can be fabricated in softer (2.5 mg/mL collagen type I assembled at 37 °C, co-culture of hMSCs and HUVECs, 1:4 ratio, 5×10^6 cells/mL), or stiffer collagen (2.5 mg/mL collagen type I assembled at 4 °C, similar cell conditions); however, the barrier function is observed mostly in the softer collagen (**G**) while stiffer conditions lead to leaky vessels (**H**) (original image)

In addition, the presence of CaP decreases the expression of genes related to pericyte differentiation [98], and mineralization decreases the differentiation of MSCs into a pericyte-like phenotype (αSMA+ cells), therefore reducing the formation of vascular capillaries in mineralized collagen scaffolds in vitro [54]. To address this issue, our group developed a cell-laden collagen hydrogel with osteoprogenitor cells, MSCs, ECs, and neural cells. Subsequently, such constructs were mineralized to mimic the intra- and extrafibrillar nanoscale mineralization profile of native bone [56••]. Differentiation of human MSCs (hMSCs) into αSMA-expressing cells in the mineralized constructs appeared to be restricted to cells in immediate contact with endothelial capillaries. On the other hand, hMSCs that appeared to be away from the forming vessels maintained their capacity to differentiate into osteoblasts, as indicated by the expression of RUXN2 in the cells (Fig. 5). This work demonstrated that an engineered 3D microenvironment that shares the hallmarks of native bone is sufficient to stimulate the osteogenic differentiation of hMSCs, while also enabling the formation of hMSC-supported vascular capillaries both in vitro and in vivo [56••].

Another important factor to consider for engineering pericyte-supported vasculature is the variable potential demonstrated by different cell sources or populations of MSCs differentiating into pericyte-like cells in engineered constructs [50, 99]. Tissue-resident MSCs isolated from the bone marrow, adipose tissue, skeletal muscle, and myocardium are known to be capable of modulating the formation of vasculature [100–103]. Fibroblasts and pericytes seem to present different functional roles in the formation of tissue-engineered microvascular networks. While fibroblasts tend to support vessel formation mostly via paracrine signaling, pericytes also contribute with direct cell-cell interactions, favoring vessel contractility [94] (Fig. 6). Conversely, for craniofacial regeneration, our group demonstrated that bone marrow MSCs are more effective in differentiating into pericyte-like cells (SMA+/NG2+) in a co-culture with HUVECs than dental pulp stem cells (hDPSCs) or stem cells from apical papilla (SCAPs) [50].

In native tissues, the EC-pericyte ratio varies across tissues. The density depends on the organ's specific functions and need for a stricter control of the endothelial barrier function. For instance, vessels in the lower torso and legs tend to have more pericytes, since they need to pump blood flow back to the heart [80]. The retina and brain have the highest density of pericytes in the human body (1:1) to provide non-leaky vessels in the eye and develop the blood-brain barrier (BBB) complex. In the lung, where vessels need to provide some permeability for gaseous exchanges, the endothelial cell/pericyte ratio is 10:1 [3, 6], and in the skeletal muscle, the ratio is 100:1. To engineer pericyte-supported vasculature, the EC/pericyte ratio can vary from 1:1 to 10:1 [50, 52, 55, 59, 100, 104, 105]. Lower ratios result in leaky vessels without barrier function.

In the literature, there are different approaches to using growth factors to promote the maturation of the vasculature. One approach is based only on the co-culture of HUVECs and MSCs to promote the differentiation of pericyte or pericyte-like cells to form mature capillaries after a few days [50, 56••,
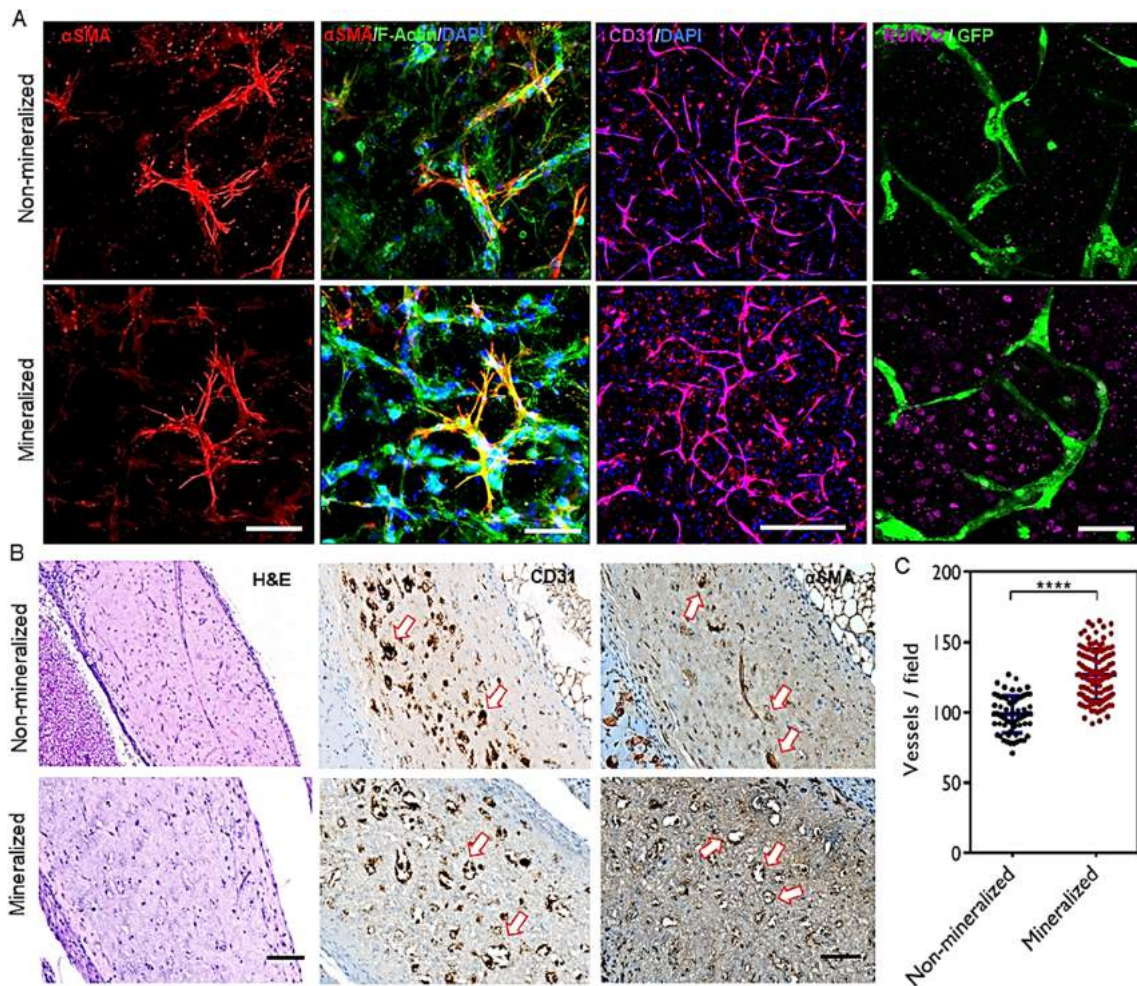
Fig. 5 Vascularization of mineralized cell-laden collagen. **A** HUVECs formed endothelial networks that were supported by αSMA-expressing hMSCs (scale bar: 50 μm) and were also positive for CD31 (scale bar: 400 μm). The remainder of hMSCs expressed RUNX2 as a marker for osteogenic differentiation (scale bar: 50 μm). **B** After 7 days of in vitro culture and 7 days of implantation, H&E images depicted the collagenous matrix populated with cells. Anti-human CD31 antibody staining (middle) suggests the formation of endothelial networks by the transplanted HUVECs as opposed to murine vasculature infiltration. Vessels in non-mineralized sections had constricted lumens (arrows), as opposed to wider HUVEC-lined vessel structures in the mineralized construct (arrows). Anti-αSMA staining (right) shows fewer αSMA+ cells in the non-mineralized sections than in the mineralized constructs, which appear to be wrapped by pericyte-like cells. Quantification of vessel numbers indicate robust vascularization and cell survival in mineralized groups, compared with their non-mineralized controls. Reproduced with permission from Thrivikraman et al. [56**]

97]. On the other hand, Jeon et al. observed a significant increase in the amount of αSMA+ cells in microvascular networks with added VEGF and transforming growth factor β1 (TGF β1) or VEGF and angiopoietin 1 (Ang-1) compared to networks with added VEGF alone. While the addition of TGF-β1 generated a non-interconnected microvasculature, Ang-1 promoted functional networks [106]. Later, this combination of endothelial-mesenchymal stem cell co-culture and the external addition of stabilizing molecules, such as an association of Ang-1 and VEGF, was used to promote the generation of functional microvascular networks, which represent a suitable model to study cancer cell extravasation [107]. Angiopoietin-1 (Ang-1) represents a key molecule in vessel stabilization and could play a role in the recruitment of mesenchymal cells in engineered vessels.

Perspectives

For a long time, pericytes were thought to only function in the trophic support of endothelial cells and in the maintenance of vasculature stabilization [13]. Occupying a strategic position between the blood stream and the interstitial space, pericytes are able to sense environmental cues from both sides in an organ-specific manner [108]. As we summarize in this review, this perspective of a so-called supportive role of pericytes has evolved to an acknowledged multipotent ability to orchestrate a great part of tissue homeostasis.

The lack of specific markers for pericytes has long been a challenge to studying these cells. CRISPR technologies associated with lineage tracing have become crucial in disclosing the continuum of changes that pericytes and their progeny go
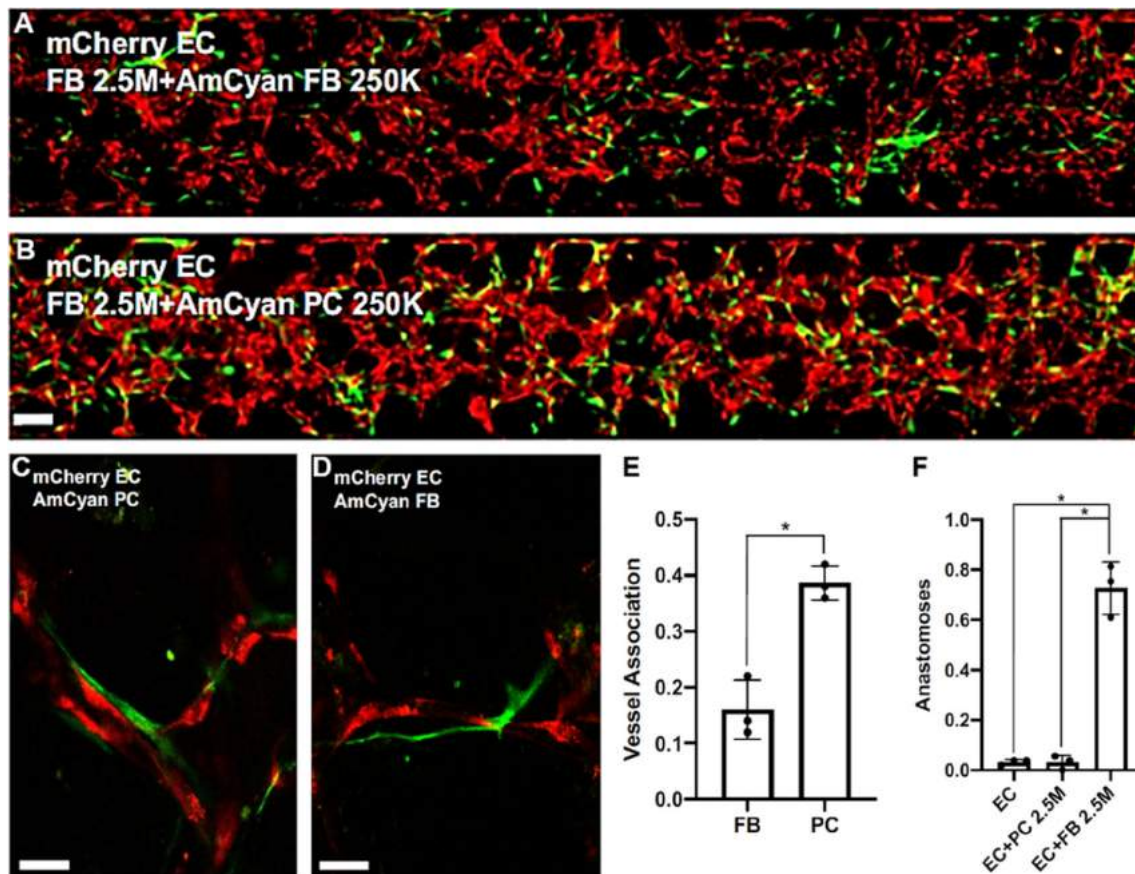
Fig. 6 Comparison of fibroblasts and pericytes in microvasculature formation using a microfluidic device. Microfluidic devices cultured for 7 days with EC-fibroblast (**A**, **D**) or EC-pericytes. **B**, **C** Pericytes are closely associated with endothelial cells (**C**, **E**) and reduced the lumen diameter (**B**) and number of anastomosis of microvessels (**F**). Reproduced with permission from Kosyakova et al. [94]

through during homeostasis, disease, and integration of engineered constructs with the host [61]. Such cell tracking strategies, allied with intravital microscopy [72•, 85, 109], provide the investigative platforms necessary to address questions that were intangible thus far. For example, cellular neighborhoods are defined as repeatable units of different cell types found in tissues, in which some structures and cells are tissue-specific and others are conserved across different tissues [110]. Considering the tissue specificity of pericytes, in vivo cell tracking tools could help determine the biomechanical properties of scaffolds to precisely control pericytes' plasticity while providing vessel stabilization as needed for each organ in a more tailored approach, instead of using pericytes as a "one-size-fits-all" type of cell. On the other hand, because pericytes are closely related to fibrosis [14, 73, 111], the use of gene editing and cell line tracking in preclinical models could provide crucial information about parameters in the scaffold design necessary to prevent engineered pericytes from contributing to tissue fibrosis instead of regeneration. Moreover, it has been shown that different stromal cell types provide different functions in microvessel assembly by endothelial cells [94]. Cell tracking strategies could help us understand if constructs intended for tissue regeneration would present a faster and more effective

integration if the engineered pericytes matched the same embryologic origin as the host.

In the literature, there is an apparent dichotomic approach to the use of pericytes in tissue engineering; the cells can be used either as vessel stabilizers [8, 100, 112] or as sources of other cell types [24••, 25, 35, 40]. Our group [54, 55, 56••, 113] and others [51, 85, 93] have shown that pericytes are multifunctional cells that, under precisely tailored and favorable conditions, can promote long-lasting vessels capable of anastomosing with the host, while a fraction of those cells can migrate away from vessels and differentiate into fibroblasts or into a mineralizing phenotype to help regenerate the tissue.

Another major problem to be addressed is how to scale up engineering strategies using pericyte-supported vasculature and how to control spatially organized vascular networks in thick cell-laden constructs [86]. A rational design of biomaterials to combine different modalities for niche manipulation could be a powerful strategy to hone pericytes' capabilities to proliferate and differentiate while supporting vasculature, minimizing the need for an unfeasible number of transplanted cells into the construct [13].

Recently, some of the immunologic functions of pericytes in guiding the innate immune cells into and outside the

intravascular space have gained more attention [114], but the understanding of how this immunologic function can be used in tissue engineering to favor an accelerated integration of an engineered construct with the host has still to be addressed. Moreover, the role of pericytes in mechanisms of immune tolerance and evasion associated with biomaterials is yet to be defined [108].

As the world population ages, more and more patients in need for engineered soft tissues and bone tissue will be experiencing senescence, which is fundamentally linked to decreased tissue repair, decreased tissue regeneration, and increased fibrosis [115, 116]. There is a large body of evidence that pericytes are involved in tissue fibrosis, along with fibroblasts and macrophages [14, 73, 111]. Some open questions related to the use of pericytes in tissue engineering are associated with the effect of an aging host on the fate of engineered pericyte-laden constructs. For example, if a pericyte-laden construct is implanted in a patient, would the senescent signals from the host impair pericyte function and shift the differentiation of the cells in the construct toward a more fibrotic, undesirable outcome? Could pericytes be potential targets for senolytic agents capable of delaying vessel regression and fibrosis in aging individuals to improve integration?

Therefore, we need to approach the use of pericytes in tissue engineering with a more comprehensive perspective to develop rationally designed biomaterials and to push the field forward.

Conclusions

In conclusion, pericytes may support the regeneration of vascularized tissues, fostering the neovascularization of the affected area by activating processes of cell proliferation, differentiation, and integration into the host tissue along with paracrine mechanisms via the secretion of growth factors and signaling molecules. Despite the large body of work on the subject, further investigation is essential to detailing the specific role of pericytes in the anastomosis of engineered host vessels and to offering potential biomolecular strategies for accelerating in vivo integration.

Declarations

Conflict of Interest The authors declare no competing interests.

Human and Animal Rights and Informed Consent This article does not contain any studies with human or animal subjects performed by any of the authors.

References

Papers of particular interest, published recently, have been highlighted as:
• Of importance
•• Of major importance

1.• Armulik A, Genove G, Betsholtz C. Pericytes: developmental, physiological, and pathological perspectives, problems, and promises. Dev Cell. 2011;21(2):193-215. **Comprehensive review about pericytes.**

2. Gaengel K, Genove G, Armulik A, Betsholtz C. Endothelial-mural cell signaling in vascular development and angiogenesis. Arterioscler Thromb Vasc Biol. 2009;29(5):630–8.

3. von Tell D, Armulik A, Betsholtz C. Pericytes and vascular stability. Exp Cell Res. 2006;312(5):623–9.

4. Allt G, Lawrenson JG. Pericytes: cell biology and pathology. Cells Tissues Organs. 2001;169(1):1–11.

5. Sims DE, Westfall JA. Analysis of relationships between pericytes and gas exchange capillaries in neonatal and mature bovine lungs. Microvasc Res. 1983;25(3):333–42.

6. Díaz-Flores L, Gutiérrez R, Madrid JF, Varela H, Valladares F, Acosta E, Martín-Vasallo P, Díaz-Flores L Jr. Pericytes. Morphofunction, interactions and pathology in a quiescent and activated mesenchymal cell niche. Histol Histopathol. 2009;24(7):909–69.

7. Bergers G, Song S. The role of pericytes in blood-vessel formation and maintenance. Neuro-Oncology. 2005;7(4):452–64.

8. Gerhardt H, Betsholtz C. Endothelial-pericyte interactions in angiogenesis. Cell Tissue Res. 2003;314(1):15–23.

9. Díaz-Flores L, Valladares F, Gutierrez R, Varela H. The role of the pericytes of the adventitial microcirculation in the arterial intimal thickening. Histol Histopathol. 1990;5(2):145–53.

10. Edelman DA, Jiang Y, Tyburski J, Wilson RF, Steffes C. Toll-like receptor-4 message is up-regulated in lipopolysaccharide-exposed rat lung pericytes. J Surg Res. 2006;134(1):22–7.

11. Chang WG, Andrejecsk JW, Kluger MS, Saltzman WM, Pober JS. Pericytes modulate endothelial sprouting. Cardiovasc Res. 2013;100(3):492–500.

12. van Hinsbergh VW, Koolwijk P. Endothelial sprouting and angiogenesis: matrix metalloproteinases in the lead. Cardiovasc Res. 2008;78(2):203–12.

13. Sá da Bandeira D, Casamitjana J, Crisan M. Pericytes, integral components of adult hematopoietic stem cell niches. Pharmacol Ther. 2017;171:104-13.

14. Birbrair A, Zhang T, Files DC, Mannava S, Smith T, Wang ZM, Messi ML, Mintz A, Delbono O. Type-1 pericytes accumulate after tissue injury and produce collagen in an organ-dependent manner. Stem Cell Res Ther. 2014;5(6):122.

15. Stark K, Eckart A, Haidari S, Tirniceriu A, Lorenz M, von Bruhl ML, et al. Capillary and arteriolar pericytes attract innate leukocytes exiting through venules and 'instruct' them with pattern-recognition and motility programs. Nat Immunol. 2013;14(1):41–51.

16. Kim JA, Tran ND, Li Z, Yang F, Zhou W, Fisher MJ. Brain endothelial hemostasis regulation by pericytes. J Cereb Blood Flow Metab. 2006;26(2):209–17.

17. Corselli M, Crisan M, Murray IR, West CC, Scholes J, Codrea F, Khan N, Péault B. Identification of perivascular mesenchymal stromal/stem cells by flow cytometry. Cytometry A. 2013;83(8): 714–20.

18. Crisan M, Yap S, Casteilla L, Chen CW, Corselli M, Park TS, Andriolo G, Sun B, Zheng B, Zhang L, Norotte C, Teng PN, Traas J, Schugar R, Deasy BM, Badylak S, Bűhring HJ, Giacobino JP, Lazzari L, et al. A perivascular origin for mesenchymal stem cells in multiple human organs. Cell Stem Cell. 2008;3(3):301–13.

19. Adams RH, Alitalo K. Molecular regulation of angiogenesis and lymphangiogenesis. Nat Rev Mol Cell Biol. 2007;8(6):464–78.

20. Sweeney M, Foldes G. It takes two: endothelial-perivascular cell cross-talk in vascular development and disease. Front Cardiovasc Med. 2018;5:154.

21. Eilken HM, Dieguez-Hurtado R, Schmidt I, Nakayama M, Jeong HW, Arf H, et al. Pericytes regulate VEGF-induced endothelial sprouting through VEGFR1. Nat Commun. 2017;8(1):1574.

22. Davies MG. Critical limb ischemia: cell and molecular therapies for limb salvage. Methodist Debakey Cardiovasc J. 2012;8(4):20–7.

23. Birbrair A, Borges IDT, Gilson Sena IF, Almeida GG, da Silva ML, Gonçalves R, et al. How plastic are pericytes? Stem Cells Dev. 2017;26(14):1013–9.

24.•• James AW, Zara JN, Zhang X, Askarinam A, Goyal R, Chiang M, et al. Perivascular stem cells: a prospectively purified mesenchymal stem cell population for bone tissue engineering. Stem Cells Transl Med. 2012;1(6):510-9. **In this study, the authors purified human perivascular stem cells (PSCs) from adipose tissue and compared their bone-forming capacity with that of traditionally derived stromal vascular fraction cells finding that PSCs undergo osteogenic differentiation in vitro and forming bone after intramuscular implantation in vivo without the need for predifferentiation.**

25. James AW, Peault B. Perivascular mesenchymal progenitors for bone regeneration. J Orthop Res. 2019;37(6):1221–8.

26. Xu J, Li D, Hsu CY, Tian Y, Zhang L, Wang Y, Tower RJ, Chang L, Meyers CA, Gao Y, Broderick K, Morris C, Hooper JE, Nimmagadda S, Péault B, James AW. Comparison of skeletal and soft tissue pericytes identifies CXCR4. Bone Res. 2020;8(1):22.

27. Hellstrom M, Kalen M, Lindahl P, Abramsson A, Betsholtz C. Role of PDGF-B and PDGFR-beta in recruitment of vascular smooth muscle cells and pericytes during embryonic blood vessel formation in the mouse. Development. 1999;126(14):3047–55.

28. Avolio E, Alvino VV, Ghorbel MT, Campagnolo P. Perivascular cells and tissue engineering: current applications and untapped potential. Pharmacol Ther. 2017;171:83–92.

29. Smyth LCD, Rustenhoven J, Scotter EL, Schweder P, Faull RLM, Park TIH, Dragunow M. Markers for human brain pericytes and smooth muscle cells. J Chem Neuroanat. 2018;92:48–60.

30. Murray IR, West CC, Hardy WR, James AW, Park TS, Nguyen A, Tawonsawatruk T, Lazzari L, Soo C, Péault B. Natural history of mesenchymal stem cells, from vessel walls to culture vessels. Cell Mol Life Sci. 2014;71(8):1353–74.

31. Hardy WR, Moldovan NI, Moldovan L, Livak KJ, Datta K, Goswami C, Corselli M, Traktuev DO, Murray IR, Péault B, March K. Transcriptional networks in single perivascular cells sorted from human adipose tissue reveal a hierarchy of mesenchymal stem cells. Stem Cells. 2017;35(5):1273–89.

32. Yamazaki T, Mukouyama YS. Tissue specific origin, development, and pathological perspectives of pericytes. Front Cardiovasc Med. 2018;5:78.

33. Wang Z, Xu Q, Zhang N, Du X, Xu G, Yan X. CD146, from a melanoma cell adhesion molecule to a signaling receptor. Signal Transduct Target Ther. 2020;5(1):148.

34. Chen J, Luo Y, Huang H, Wu S, Feng J, Zhang J, Yan X. CD146 is essential for PDGFRβ-induced pericyte recruitment. Protein Cell. 2018;9(8):743–7.

35. James AW, Hindle P, Murray IR, West CC, Tawonsawatruk T, Shen J, Asatrian G, Zhang X, Nguyen V, Simpson AH, Ting K, Péault B, Soo C. Pericytes for the treatment of orthopedic conditions. Pharmacol Ther. 2017;171:93–103.

36. Wang Y, Xu J, Chang L, Meyers CA, Zhang L, Broderick K, Lee M, Peault B, James AW. Relative contributions of adipose-resident CD146(+) pericytes and CD34(+) adventitial progenitor cells in bone tissue engineering. NPJ Regen Med. 2019;4:1.

37. Xu J, Wang Y, Gomez-Salazar MA, Hsu GC, Negri S, Li Z, et al. Bone-forming perivascular cells: Cellular heterogeneity and use for tissue repair. Stem Cells. 2021;39:1427–34.

38. Yao Q, Wei B, Liu N, Li C, Guo Y, Shamie AN, Chen J, Tang C, Jin C, Xu Y, Bian X, Zhang X, Wang L. Chondrogenic regeneration using bone marrow clots and a porous polycaprolactone-hydroxyapatite scaffold by three-dimensional printing. Tissue Eng Part A. 2015;21(7-8):1388–97.

39. Meyers CA, Xu J, Zhang L, Chang L, Wang Y, Asatrian G, Ding C, Yan N, Zou E, Broderick K, Lee M, Peault B, James AW. Skeletogenic capacity of human perivascular stem cells obtained via magnetic-activated cell sorting. Tissue Eng Part A. 2019;25(23-24):1658–66.

40. Meyers CA, Casamitjana J, Chang L, Zhang L, James AW, Peault B. Pericytes for therapeutic bone repair. Adv Exp Med Biol. 2018;1109:21–32.

41. Hsu GC, Cherief M, Sono T, Wang Y, Negri S, Xu J, et al. Divergent effects of distinct perivascular cell subsets for intra-articular cell therapy in posttraumatic osteoarthritis. J Orthop Res. 2021;39:2388–97.

42. Lee YH, Petkova AP, Mottillo EP, Granneman JG. In vivo identification of bipotential adipocyte progenitors recruited by β3-adrenoceptor activation and high-fat feeding. Cell Metab. 2012;15(4):480–91.

43. Maki T, Maeda M, Uemura M, Lo EK, Terasaki Y, Liang AC, Shindo A, Choi YK, Taguchi A, Matsuyama T, Takahashi R, Ihara M, Arai K. Potential interactions between pericytes and oligodendrocyte precursor cells in perivascular regions of cerebral white matter. Neurosci Lett. 2015;597:164–9.

44. Farahani RM, Xaymardan M. Platelet-derived growth factor receptor alpha as a marker of mesenchymal stem cells in development and stem cell biology. Stem Cells Int. 2015;2015:362753.

45. Wang Y, Xu J, Meyers CA, Gao Y, Tian Y, Broderick K, Peault B, James AW. PDGFRalpha marks distinct perivascular populations with different osteogenic potential within adipose tissue. Stem Cells. 2020;38(2):276–90.

46. Fukushi J, Makagiansar IT, Stallcup WB. NG2 proteoglycan promotes endothelial cell motility and angiogenesis via engagement of galectin-3 and alpha3beta1 integrin. Mol Biol Cell. 2004;15(8): 3580–90.

47. Ozerdem U, Stallcup WB. Early contribution of pericytes to angiogenic sprouting and tube formation. Angiogenesis. 2003;6(3): 241–9.

48. Schlingemann RO, Rietveld FJ, de Waal RM, Ferrone S, Ruiter DJ. Expression of the high molecular weight melanoma-associated antigen by pericytes during angiogenesis in tumors and in healing wounds. Am J Pathol. 1990;136(6):1393–405.

49. Murfee WL, Skalak TC, Peirce SM. Differential arterial/venous expression of NG2 proteoglycan in perivascular cells along microvessels: identifying a venule-specific phenotype. Microcirculation. 2005;12(2):151–60.

50. Parthiban SP, He W, Monteiro N, Athirasala A, França CM, Bertassoni LE. Engineering pericyte-supported microvascular capillaries in cell-laden hydrogels using stem cells from the bone marrow, dental pulp and dental apical papilla. Sci Rep. 2020;10(1):21579.

51. Cheng G, Liao S, Kit Wong H, Lacorre DA, di Tomaso E, Au P, Fukumura D, Jain RK, Munn LL. Engineered blood vessel networks connect to host vasculature via wrapping-and-tapping anastomosis. Blood. 2011;118(17):4740–9.

52. Kusuma S, Shen YI, Hanjaya-Putra D, Mali P, Cheng L, Gerecht S. Self-organized vascular networks from human pluripotent stem cells in a synthetic matrix. Proc Natl Acad Sci U S A. 2013;110(31):12601–6.

53. Sakuma R, Kawahara M, Nakano-Doi A, Takahashi A, Tanaka Y, Narita A, Kuwahara-Otani S, Hayakawa T, Yagi H, Matsuyama T, Nakagomi T. Brain pericytes serve as microglia-generating multipotent vascular stem cells following ischemic stroke. J Neuroinflammation. 2016;13(1):57.

54. Franca CM, Thrivikraman G, Athirasala A, Tahayeri A, Gower LB, Bertassoni LE. The influence of osteopontin-guided collagen intrafibrillar mineralization on pericyte differentiation and vascularization of engineered bone scaffolds. J Biomed Mater Res B Appl Biomater. 2018.

55. Subbiah R, Thrivikraman G, Parthiban SP, Jones JM, Athirasala A, Xie H, Bertassoni LE. Prevascularized hydrogels with mature vascular networks promote the regeneration of critical-size calvarial bone defects in vivo. J Tissue Eng Regen Med. 2021;15(3):219–31.

56.•• Thrivikraman G, Athirasala A, Gordon R, Zhang L, Bergan R, Keene DR, et al. Rapid fabrication of vascularized and innervated cell-laden bone models with biomimetic intrafibrillar collagen mineralization. Nat Commun. 2019;10(1):3520. **This work demonstrated the key properties of an engineered bone mimetic tissue necessary to stimulate the osteogenic differentiation of hMSCs, while also enabling the formation of pericyte-supported vascular capillaries without the addition of growth factors both in-vitro and in-vivo.**

57. Alimperti S, Mirabella T, Bajaj V, Polacheck W, Pirone DM, Duffield J, Eyckmans J, Assoian RK, Chen CS. Three-dimensional biomimetic vascular model reveals a RhoA, Rac1, and. Proc Natl Acad Sci U S A. 2017;114(33):8758–63.

58. Ben-Shaul S, Landau S, Merdler U, Levenberg S. Mature vessel networks in engineered tissue promote graft-host anastomosis and prevent graft thrombosis. Proc Natl Acad Sci U S A. 2019;116(8):2955–60.

59. Kim J, Chung M, Kim S, Jo DH, Kim JH, Jeon NL. Engineering of a biomimetic pericyte-covered 3D microvascular network. PLoS ONE. 2015;10(7):e0133880.

60. Kramann R, Schneider RK, DiRocco DP, Machado F, Fleig S, Bondzie PA, et al. Perivascular Gli1+ progenitors are key contributors to injury-induced organ fibrosis. Cell Stem Cell. 2015;16(1):51–66.

61. Galat Y, Gu H, Perepitchka M, Taylor R, Yoon JW, Glukhova XA, Li XN, Beletsky IP, Walterhouse DO, Galat V, Iannaccone PM. CRISPR editing of the GLI1 first intron abrogates GLI1 expression and differentially alters lineage commitment. Stem Cells. 2021;39(5):564–80.

62. Kramann R, Goettsch C, Wongboonsin J, Iwata H, Schneider RK, Kuppe C, Kaesler N, Chang-Panesso M, Machado FG, Gratwohl S, Madhurima K, Hutcheson JD, Jain S, Aikawa E, Humphreys BD. Adventitial MSC-like cells are progenitors of vascular smooth muscle cells and drive vascular calcification in chronic kidney disease. Cell Stem Cell. 2016;19(5):628–42.

63. Baker AH, Péault B. A Gli(1)ttering role for perivascular stem cells in blood vessel remodeling. Cell Stem Cell. 2016;19(5):563–5.

64. Park S, Zhao H, Urata M, Chai Y. Sutures possess strong regenerative capacity for calvarial bone injury. Stem Cells Dev. 2016;25(23):1801–7.

65. Dias DO, Kalkitsas J, Kelahmetoglu Y, Estrada CP, Tatarishvili J, Holl D, Jansson L, Banitalebi S, Amiry-Moghaddam M, Ernst A, Huttner HB, Kokaia Z, Lindvall O, Brundin L, Frisén J, Göritz C. Pericyte-derived fibrotic scarring is conserved across diverse central nervous system lesions. Nat Commun. 2021;12(1):5501.

66. Dias Moura Prazeres PH, Sena IFG, Borges IDT, de Azevedo PO, Andreotti JP, de Paiva AE, et al. Pericytes are heterogeneous in their origin within the same tissue. Dev Biol. 2017;427(1):6–11.

67. Göritz C, Dias DO, Tomilin N, Barbacid M, Shupliakov O, Frisén J. A pericyte origin of spinal cord scar tissue. Science. 2011;333(6039):238–42.

68. Birbrair A, Zhang T, Wang ZM, Messi ML, Mintz A, Delbono O. Type-1 pericytes participate in fibrous tissue deposition in aged skeletal muscle. Am J Physiol Cell Physiol. 2013;305(11):C1098–113.

69. Birbrair A, Zhang T, Wang ZM, Messi ML, Enikolopov GN, Mintz A, Delbono O. Role of pericytes in skeletal muscle regeneration and fat accumulation. Stem Cells Dev. 2013;22(16):2298–314.

70. Zhu S, Chen M, Ying Y, Wu Q, Huang Z, Ni W, Wang X, Xu H, Bennett S, Xiao J, Xu J. Versatile subtypes of pericytes and their roles in spinal cord injury repair, bone development and repair. Bone Res. 2022;10(1):30.

71. Shi S, Gronthos S. Perivascular niche of postnatal mesenchymal stem cells in human bone marrow and dental pulp. J Bone Miner Res. 2003;18(4):696–704.

72.• Guimaraes-Camboa N, Cattaneo P, Sun Y, Moore-Morris T, Gu Y, Dalton ND, et al. Pericytes of multiple organs do not behave as mesenchymal stem cells in vivo. Cell Stem Cell. 2017;20(3):345-59 e5. **In this paper the authors challenge the current view of endogenous pericytes as multipotent tissue-resident progenitors and suggest that the plasticity observed in vitro or following transplantation in vivo arises from artificial cell manipulations ex vivo.**

73. Thomas H, Cowin AJ, Mills SJ. The importance of pericytes in healing: wounds and other pathologies. Int J Mol Sci. 2017;18(6).

74. Farrington-Rock C, Crofts NJ, Doherty MJ, Ashton BA, Griffin-Jones C, Canfield AE. Chondrogenic and adipogenic potential of microvascular pericytes. Circulation. 2004;110(15):2226–32.

75. Brighton CT, Lorich DG, Kupcha R, Reilly TM, Jones AR, Woodbury RA. The pericyte as a possible osteoblast progenitor cell. Clin Orthop Relat Res. 1992;275:287–99.

76. Dayoub S, Devlin H, Sloan P. Evidence for the formation of metaplastic bone from pericytes in calcifying fibroblastic granuloma. J Oral Pathol Med. 2003;32(4):232–6.

77. Kirton JP, Crofts NJ, George SJ, Brennan K, Canfield AE. Wnt/beta-catenin signaling stimulates chondrogenic and inhibits adipogenic differentiation of pericytes: potential relevance to vascular disease? Circ Res. 2007;101(6):581–9.

78. Chamberlain MD, Gupta R, Sefton MV. Bone marrow-derived mesenchymal stromal cells enhance chimeric vessel development driven by endothelial cell-coated microtissues. Tissue Eng Part A. 2012;18(3-4):285–94.

79. Chung CG, James AW, Asatrian G, Chang L, Nguyen A, Le K, et al. Human perivascular stem cell-based bone graft substitute induces rat spinal fusion. Stem Cells Transl Med. 2014;3(10):1231–41.

80. Sims DE. Diversity within pericytes. Clin Exp Pharmacol Physiol. 2000;27(10):842–6.

81. Tawonsawatruk T, West CC, Murray IR, Soo C, Peault B, Simpson AH. Adipose derived pericytes rescue fractures from a failure of healing–non-union. Sci Rep. 2016;6:22779.

82. Avolio E, Rodriguez-Arabaolaza I, Spencer HL, Riu F, Mangialardi G, Slater SC, Rowlinson J, Alvino VV, Idowu OO, Soyombo S, Oikawa A, Swim MM, Kong CHT, Cheng H, Jia H, Ghorbel MT, Hancox JC, Orchard CH, Angelini G, et al. Expansion and characterization of neonatal cardiac pericytes provides a novel cellular option for tissue engineering in congenital heart disease. J Am Heart Assoc. 2015;4(6):e002043.

83. Dellavalle A, Maroli G, Covarello D, Azzoni E, Innocenzi A, Perani L, Antonini S, Sambasivan R, Brunelli S, Tajbakhsh S, Cossu G. Pericytes resident in postnatal skeletal muscle differentiate into muscle fibres and generate satellite cells. Nat Commun. 2011;2:499.

84. Sacchetti B, Funari A, Remoli C, Giannicola G, Kogler G, Liedtke S, Cossu G, Serafini M, Sampaolesi M, Tagliafico E, Tenedini E, Saggio I, Robey PG, Riminucci M, Bianco P. No identical "mesenchymal stem cells" at different times and sites: human committed progenitors of distinct origin and differentiation potential are incorporated as adventitial cells in microvessels. Stem Cell Rep. 2016;6(6):897–913.

85. Koike N, Fukumura D, Gralla O, Au P, Schechner JS, Jain RK. Tissue engineering: creation of long-lasting blood vessels. Nature. 2004;428(6979):138–9.

86. Barabaschi GD, Manoharan V, Li Q, Bertassoni LE. Engineering pre-vascularized scaffolds for bone regeneration. Adv Exp Med Biol. 2015;881:79–94.

87. Sobhan PK, Seervi M, Joseph J, Varghese S, Pillai PR, Sivaraman DM, James J, George RE, Elizabeth KE, Santhoshkumar TR, Pillai MR. Immortalized functional endothelial progenitor cell lines from umbilical cord blood for vascular tissue engineering. Tissue Eng Part C Methods. 2012;18(11):890–902.

88. Kaigler D, Wang Z, Horger K, Mooney DJ, Krebsbach PH. VEGF scaffolds enhance angiogenesis and bone regeneration in irradiated osseous defects. J Bone Miner Res. 2006;21(5):735–44.

89. Geng Y, Duan H, Xu L, Witman N, Yan B, Yu Z, Wang H, Tan Y, Lin L, Li D, Bai S, Fritsche-Danielson R, Yuan J, Chien K, Wei M, Fu W. BMP-2 and VEGF-A modRNAs in collagen scaffold synergistically drive bone repair through osteogenic and angiogenic pathways. Commun Biol. 2021;4(1):82.

90. Subbiah R, Guldberg RE. Materials science and design principles of growth factor delivery systems in tissue engineering and regenerative medicine. Adv Healthc Mater. 2019;8(1):e1801000.

91. Subbiah R, Hipfinger C, Tahayeri A, Athirasala A, Horsophonphong S, Thrivikraman G, et al. 3D printing of microgel-loaded modular microcages as instructive scaffolds for tissue engineering. Adv Mater. 2020:e2001736.

92. Greco Song HH, Rumma RT, Ozaki CK, Edelman ER, Chen CS. Vascular tissue engineering: progress, challenges, and clinical promise. Cell Stem Cell. 2018;22(4):608.

93. Chen X, Aledia AS, Ghajar CM, Griffith CK, Putnam AJ, Hughes CC, et al. Prevascularization of a fibrin-based tissue construct accelerates the formation of functional anastomosis with host vasculature. Tissue Eng Part A. 2009;15(6):1363–71.

94. Kosyakova N, Kao DD, Figetakis M, López-Giráldez F, Spindler S, Graham M, James KJ, Won Shin J, Liu X, Tietjen GT, Pober JS, Chang WG. Differential functional roles of fibroblasts and pericytes in the formation of tissue-engineered microvascular networks in vitro. NPJ Regen Med. 2020;5:1.

95. Polacheck WJ, Kutys ML, Tefft JB, Chen CS. Microfabricated blood vessels for modeling the vascular transport barrier. Nat Protoc. 2019;14(5):1425–54.

96. Engler AJ, Sen S, Sweeney HL, Discher DE. Matrix elasticity directs stem cell lineage specification. Cell. 2006;126(4):677–89.

97. Monteiro N, He W, Franca CM, Athirasala A, Bertassoni LE. Engineering microvascular networks in LED light-cured cell-laden hydrogels. ACS Biomater Sci Eng. 2018;4(7):2563–70.

98. Twohig C, Helsinga M, Mansoorifar A, Athirasala A, Tahayeri A, França CM, Pajares SA, Abdelmoniem R, Scherrer S, Durual S, Ferracane J, Bertassoni LE. A dual-ink 3D printing strategy to engineer pre-vascularized bone scaffolds in-vitro. Mater Sci Eng C Mater Biol Appl. 2021;123:111976.

99. Xu J, Gong T, Heng BC, Zhang CF. A systematic review: differentiation of stem cells into functional pericytes. FASEB J. 2017;31(5):1775–86.

100. Lin RZ, Moreno-Luna R, Zhou B, Pu WT, Melero-Martin JM. Equal modulation of endothelial cell function by four distinct tissue-specific mesenchymal stem cells. Angiogenesis. 2012;15(3):443–55.

101. Melero-Martin JM, Khan ZA, Picard A, Wu X, Paruchuri S, Bischoff J. In vivo vasculogenic potential of human blood-derived endothelial progenitor cells. Blood. 2007;109(11):4761–8.

102. Traktuev DO, Prater DN, Merfeld-Clauss S, Sanjeevaiah AR, Saadatzadeh MR, Murphy M, Johnstone BH, Ingram DA, March KL. Robust functional vascular network formation in vivo by cooperation of adipose progenitor and endothelial cells. Circ Res. 2009;104(12):1410–20.

103. Melero-Martin JM, De Obaldia ME, Kang SY, Khan ZA, Yuan L, Oettgen P, et al. Engineering robust and functional vascular networks in vivo with human adult and cord blood-derived progenitor cells. Circ Res. 2008;103(2):194–202.

104. Xiong H, Chen K, Huang Y, Liu C. Human stem cells from apical papilla can regenerate dentin-pulp complex. Nan Fang Yi Ke Da Xue Xue Bao. 2013;33(10):1512–6.

105. Miller JS, Stevens KR, Yang MT, Baker BM, Nguyen DH, Cohen DM, et al. Rapid casting of patterned vascular networks for perfusable engineered three-dimensional tissues. Nat Mater. 2012;11(9):768–74.

106. Jeon JS, Bersini S, Whisler JA, Chen MB, Dubini G, Charest JL, Moretti M, Kamm RD. Generation of 3D functional microvascular networks with human mesenchymal stem cells in microfluidic systems. Integr Biol (Camb). 2014;6(5):555–63.

107. Jeon JS, Bersini S, Gilardi M, Dubini G, Charest JL, Moretti M, Kamm RD. Human 3D vascularized organotypic microfluidic assays to study breast cancer cell extravasation. Proc Natl Acad Sci U S A. 2015;112(1):214–9.

108. Stark K, Pekayvaz K, Massberg S. Role of pericytes in vascular immunosurveillance. Front Biosci (Landmark Ed). 2018;23:767-81.

109. Nguyen DT, Lee E, Alimperti S, Norgard RJ, Wong A, Lee JJ, et al. A biomimetic pancreatic cancer on-chip reveals endothelial ablation via ALK7 signaling. Sci Adv. 2019;5(8):eaav6789.

110. Hickey JW, Neumann EK, Radtke AJ, Camarillo JM, Beuschel RT, Albanese A, McDonough E, Hatler J, Wiblin AE, Fisher J, Croteau J, Small EC, Sood A, Caprioli RM, Angelo RM, Nolan GP, Chung K, Hewitt SM, Germain RN, et al. Spatial mapping of protein composition and tissue organization: a primer for multiplexed antibody-based imaging. Nat Methods. 2021;19:284–95.

111. Kida Y, Duffield JS. Pivotal role of pericytes in kidney fibrosis. Clin Exp Pharmacol Physiol. 2011;38(7):467–73.

112. Simonavicius N, Ashenden M, van Weverwijk A, Lax S, Huso DL, Buckley CD, Huijbers IJ, Yarwood H, Isacke CM. Pericytes promote selective vessel regression to regulate vascular patterning. Blood. 2012;120(7):1516–27.

113. Athirasala A, Lins F, Tahayeri A, Hinds M, Smith AJ, Sedgley C, Ferracane J, Bertassoni LE. A novel strategy to engineer pre-vascularized full-length dental pulp-like tissue constructs. Sci Rep. 2017;7(1):3323.

114. Stark K, Eckart A, Haidari S, Tirniceriu A, Lorenz M, von Brühl ML, Gärtner F, Khandoga AG, Legate KR, Pless R, Hepper I, Lauber K, Walzog B, Massberg S. Capillary and arteriolar pericytes attract innate leukocytes exiting through venules and

'instruct' them with pattern-recognition and motility programs. Nat Immunol. 2013;14(1):41–51.

115. Di Micco R, Krizhanovsky V, Baker D. d'Adda di Fagagna F. Cellular senescence in ageing: from mechanisms to therapeutic opportunities. Nat Rev Mol Cell Biol. 2021;22(2):75–95.

116. Tchkonia T, Zhu Y, van Deursen J, Campisi J, Kirkland JL. Cellular senescence and the senescent secretory phenotype: therapeutic opportunities. J Clin Invest. 2013;123(3):966–72.

Publisher's Note Springer Nature remains neutral with regard to jurisdictional claims in published maps and institutional affiliations.

AUTHOR QUERY

AUTHOR PLEASE ANSWER QUERY.

Q1. Panel label F was not mentioned in Figure 4 caption. Kindly check.

Apologies for the oversight. Panel F should be mentioned in the caption as:
E Single vessels can be fabricated in softer (2.5 mg/mL collagen type I assembled at 37 oC, co-culture of hMSCs and HUVECs, 1:4 ratio, 5 x 106 cells/mL) or (F) stiffer collagen (2.5 mg/mL collagen type I assembled at 4 oC, similar cell conditions)